



Probe, Sample, and Instrument (PSI): The Hat-Trick for Fluorescence Live Cell Imaging

Ludovic Galas, Thibault Gallavardin, Magalie Benard, Arnaud Lehner, Damien Schapman, Alexis Lebon, Hitoshi Komuro, Patrice Lerouge, Stéphane Leleu, Xavier Franck

► To cite this version:

Ludovic Galas, Thibault Gallavardin, Magalie Benard, Arnaud Lehner, Damien Schapman, et al.. Probe, Sample, and Instrument (PSI): The Hat-Trick for Fluorescence Live Cell Imaging. Chemosensors, 2018, 6 (3), pp.40. 10.3390/chemosensors6030040 . hal-01874039

HAL Id: hal-01874039

<https://normandie-univ.hal.science/hal-01874039>

Submitted on 6 Dec 2019

HAL is a multi-disciplinary open access archive for the deposit and dissemination of scientific research documents, whether they are published or not. The documents may come from teaching and research institutions in France or abroad, or from public or private research centers.



L'archive ouverte pluridisciplinaire **HAL**, est destinée au dépôt et à la diffusion de documents scientifiques de niveau recherche, publiés ou non, émanant des établissements d'enseignement et de recherche français ou étrangers, des laboratoires publics ou privés.



Distributed under a Creative Commons Attribution 4.0 International License

Review

“Probe, Sample, and Instrument (PSI)”: The Hat-Trick for Fluorescence Live Cell Imaging

Ludovic Galas ^{1,*}, Thibault Gallavardin ², Magalie Bénard ¹, Arnaud Lehner ³ ,
Damien Schapman ¹, Alexis Lebon ¹, Hitoshi Komuro ⁴, Patrice Lerouge ³, Stéphane Leleu ²
and Xavier Franck ² 

¹ Normandie Université, UNIROUEN, INSERM, PRIMACEN, 76000 Rouen, France; magalie.benard@univ-rouen.fr (M.B.); damien.schapman@univ-rouen.fr (D.S.); alexis.lebon@univ-rouen.fr (A.L.)

² Normandie Université, CNRS, INSA Rouen, UNIROUEN, COBRA, 76000 Rouen, France; thibault.gallavardin@univ-rouen.fr (T.G.); stephane.leleu@univ-rouen.fr (S.L.); xavier.franck@insa-rouen.fr (X.F.)

³ Normandie Université, UNIROUEN, Laboratoire Glycobiologie et Matrice Extracellulaire végétale (Glyco-MEV) EA4358, 76821 Mont-Saint-Aignan, France; arnaud.lehner@univ-rouen.fr (A.L.); patrice.lerouge@univ-rouen.fr (P.L.)

⁴ Department of Neuroscience, School of Medicine, Yale University, New Haven, CT 06510, USA; hitoshi.komuro@yale.edu

* Correspondence: ludovic.galas@univ-rouen.fr; Tel.: +33-235-14-7048

Received: 14 June 2018; Accepted: 10 September 2018; Published: 13 September 2018



Abstract: Cell Imaging Platforms (CIPs) are research infrastructures offering support to a number of scientific projects including the choice of adapted fluorescent probes for live cell imaging. What to detect in what type of sample and for how long is a major issue with fluorescent probes and, for this, the “hat-trick” “Probe–Sample–Instrument” (PSI) has to be considered. We propose here to deal with key points usually discussed in CIPs including the properties of fluorescent organic probes, the modality of cell labeling, and the best equipment to obtain appropriate spectral, spatial, and temporal resolution. New strategies in organic synthesis and click chemistry for accessing probes with enhanced photophysical characteristics and targeting abilities will also be addressed. Finally, methods for image processing will be described to optimize exploitation of fluorescence signals.

Keywords: fluorescent probes; small fluorescent organic molecules; fluorescent proteins; cell labeling; live cell imaging; photophysical properties; organic synthesis; click chemistry; advanced microscopy; instrumental performances; image processing

1. Introduction

Since the 1960s, the discovery of fluorescent proteins [1,2] has boosted live cell imaging studies and, consequently, technological developments for microscopy including simultaneous resolution improvement [3–6] and detector sensitivity [7,8]. In the early 2000s, European and also French (Infrastructure en Biologie, Santé et Agronomie, IBiSA) policies were established to identify emerging cell imaging platforms (CIPs) in which equipment, human resources, and skills are mutualized to facilitate broad access to advanced technologies. Economic reasons have also driven sharing strategies since the price for a commercial live cell imaging system starts around 100 k€ for a basic plate reader and reaches 1 M€ for a fully equipped STimulated Emission Depletion (STED) nanoscope. Frequently, CIPs are at the crossroads between molecular and cellular biology, chemistry, informatics, and engineering. By taking advantage of the diversity of projects and biological models studied on the Norman IBiSA CIP, the so-called PRIMACEN (Plate-forme de Recherche en IMagerie CELLulaire de Normandie),

we propose here the concept of the “Probe–Sample–Instrument” triad that is necessary to consider when choosing a fluorescent probe for live cell imaging (Figure 1).

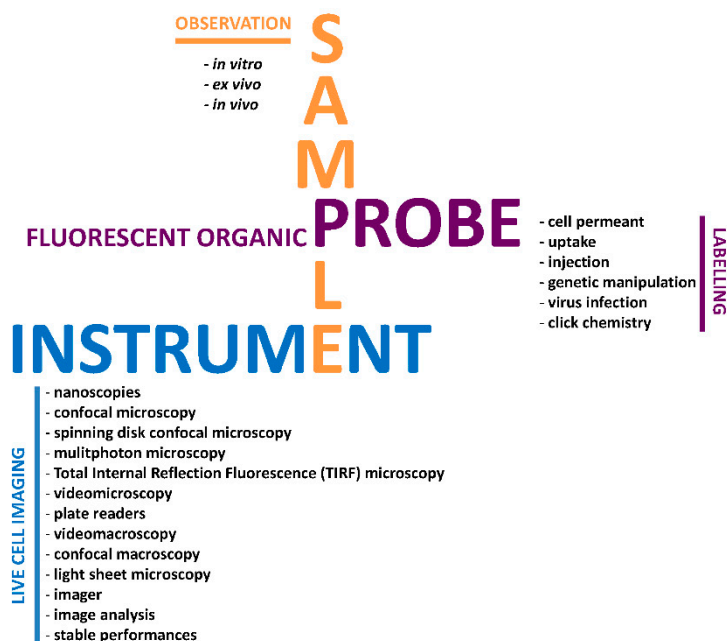


Figure 1. Representation of the “Probe–Sample–Instrument” (PSI) triad. Interrelation between the three essential key elements for successful live cell imaging. Type of sample observation, strategies for fluorescent cell labeling, and diversity of live cell imaging instruments are listed.

On one hand, there is a large diversity of chemical and biomolecular strategies to construct new fluorescent probes with enhanced properties and specificities. In this review, we will focus only on organic fluorescent dyes including small organic fluorophores and fluorescent proteins; other fluorophores such as metal complexes [9–11], lanthanide complexes [12–14] and nanoparticles [15–17], fluorescent polymers [18,19], quantum dots [20–22], carbon dots [23], and nanoparticles [24,25] will not be detailed. On the other hand, localization or tracking of molecules, organelles, or cells in living cells, tissues, or organisms, without perturbing cellular processes, is an ongoing, fascinating research area [26]. Many methods for fluorescent labeling including diffusion of cell-permeable probes [27], uptake [28,29], injection [30], chemical and enzymatic reactions [31,32], genetic manipulation [31,32], and virus transfection [33] are now available. Indeed, the final choice of the labeling strategy depends on the cellular target but also on the experimental conditions, i.e., *in vitro*, *ex vivo*, or *in vivo* studies. In addition, probes and methods of labeling should also be adapted to prokaryotes or eukaryotes and to the presence of autofluorescence, siliceous structures, or walls. Finally, for live cell imaging, a dye should be excitable with a low-power light source and be detected with high- and stable-performance equipment but should not be cytotoxic and not bleach rapidly upon irradiation [34]. From nanoscopy to light sheet microscopy, there is a large variety of imaging systems and devices with spatial and temporal resolution ranges [6,35–39]. These instruments are also adapted to the type of living sample and to the detection of low- to high-intensity signals. Therefore, photophysics of fluorescent organic probes, methods for cell and tissue labeling with a focus on click chemistry, progress in synthesis of small fluorescent organic molecules, and instrumental requirements for appropriate probe excitation and signal detection/analysis will be successively described in this review in the context of the PSI triad.

2. Photophysical Properties of Fluorescent Organic Probes

Knowledge of spectral characteristics of a fluorescent probe is undoubtedly essential to refining excitation and emission detection with corresponding instruments. With the development of advanced

light technologies including multiphoton or nanoscopies (super-resolution microscopies), it is also crucial to consider the quantum yield, the brightness, the photostability, the Stokes shift, and the cross section to determine if the probe is suitable for live cell imaging studies [40–42].

2.1. General Properties

The most significant photophysical parameters for fluorescence imaging are depicted in the Perrin–Jablonski diagram [6] (Figure 2), which presents the entire cycle that has to be considered to figure out the potential of fluorescence imaging.

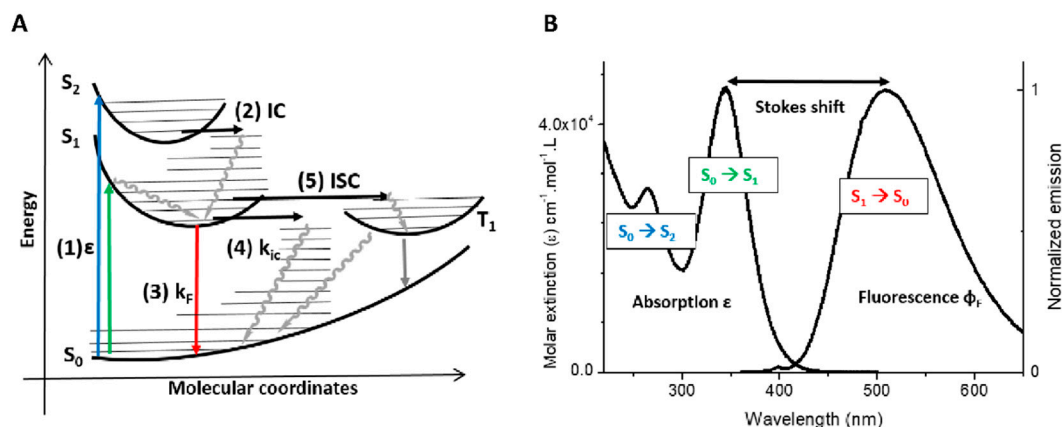


Figure 2. Photophysical parameters for fluorescent organic probes. (A) Perrin–Jablonski diagram containing three singlet states S₀, S₁, S₂ and a triplet state T₁. (B) UV–visible absorption and emission spectra. Molecular coordinates refer to molecular conformational evolution occurring during photophysical processes. ϵ molar extinction, IC internal conversion, ISC intersystem crossing, k_F fluorescence rate constant, k_{IC} internal conversion rate constant, ϕ_F fluorescence quantum yield.

Fluorescence proceeds through three successive steps, i.e., (1) absorption of a photon to reach nonstabilized excited states (Franck Condon states), (2) stabilization of the excited state by vibrational relaxation and internal conversion (IC) to populate the lowest excited state (Kasha State), and (3) radiative decay resulting in the emission of a photon. The absorption efficiency is described by the molar extinction coefficient ϵ defined by the Beer–Lambert law (Equation (1)). The ϵ value ranges from $10^4 \text{ cm}^{-1} \cdot \text{mol}^{-1} \cdot \text{L}$, for the less absorbing chromophores, to 10^6 for the commonly used fluorophores, depending of the nature of the transition involved.

$$A = \epsilon(\lambda)lc \quad (1)$$

In Equation (1), A is the absorbance as a function of $\epsilon(\lambda)$, the molar extinction coefficient; l is the cuvette length in cm; and c is the concentration of the chromophore.

As the absorption process is extremely fast ($<10^{-15} \text{ s}$) [42], the molecules are considered motionless during the process leading to transient excited states (Figure 2A, Step 1). These states feature the same conformation as fundamental states but with distinct molecular orbital configurations. They quickly stabilize by vibrational relaxation leading to conformation change and then to internal conversion (Figure 2A, Step 2) to the lowest excited energy state from which fluorescence will arise (Figure 2A, Step 3). The efficiency of the emission process is described by the fluorescence quantum yield (ϕ_F), which is the ratio between the number of emitted and absorbed photons ($0 < \phi_F < 1$; Equation (2)). Indeed, the excited state may also decay through nonradiative processes such as internal conversion (IC) (Figure 2A, Step 4), resulting in heat release or intersystem crossing (ISC) (Figure 2A, Step 5) to populate the triplet state (T₁).

$$\phi_F = \frac{k_F}{k_F + k_{IC} + k_{ISC}} \quad (2)$$

Equation (2) shows fluorescence quantum yield as a function of the deactivation kinetics of the excited state; subscript F denotes fluorescence, IC denotes internal conversion, and ISC denotes intersystem crossing.

The “Kasha rule” states that fluorescence arises only from the lowest excited state of singlet spin multiplicity; therefore, the emission spectrum and quantum yield do not depend on the excitation wavelength, as higher states decay to the lowest excited state. It also implies that a fluorophore features only one fluorescence band arising from the “Kasha state”. The overall efficiency of a fluorophore can be represented using the brightness β accounting for the ability to both absorb and emit photons (Equation (3)).

$$\beta = \varepsilon(\lambda) \times \varphi_F \quad (3)$$

Equation (3) gives the brightness as a function of $\varepsilon(\lambda)$ and φ_F .

The absorption and emission spectra also give access to another property: the “Stokes shift”, which is the difference between the absorption band of higher wavelength and the emission band (Figure 2B). The Stokes shift corresponds also to the energy difference between absorption and emission caused by the stabilization of the excited state before emission; it has to be expressed in cm^{-1} or eV (Equation (4)) to compare the energy of absorption and emission at different wavelengths, since wavelength is inversely proportional to energy. This property is also important in fluorescence microscopy; in this case, the direct wavelength difference in nanometers is more convenient to define the emission and the absorption spectral windows.

$$\Delta\nu_{\text{stokes}} = \tilde{\nu}_{\text{abs}} - \tilde{\nu}_{\text{em}} = 1/\lambda_{\text{abs}} - 1/\lambda_{\text{em}} \quad (4)$$

Equation (4) gives the Stokes shift expressed in cm^{-1} ; $\tilde{\nu}_{\text{abs}}$ and $\tilde{\nu}_{\text{em}}$ correspond to absorption and emission wavenumber.

The Stokes shift is very significant in terms of the photophysical properties of a fluorophore: A small Stokes shift means that the electron density of the excited state is similar to that of the fundamental state. A large Stokes shift is evidence of a strong reorganization and stabilization of the chromophores at its excited state due to environmental or internal effects.

2.2. Small Organic Fluorophore Classification and Structure–Fluorescence Relationship

A classification to briefly outline the nature of the most common fluorescence transitions in relation to the structure of small organic fluorophores can be established (Figure 3):

- **Apolar chromophores** in which local state emission occurs with no electron donor and accepting groups. Due to this absence, electrons remain localized at the excited state. Local state emission features small Stokes shifts, and can present vibronic structures and symmetry if the π -conjugated system is very rigid. The most common apolar fluorophores are perylenes, anthracenes, rubrenes, and pyrenes.
- **Push–pull chromophores** possessing strong electron donor and accepting groups. These groups favor electron delocalization along all of the π -conjugated system, leading to significant electron density change or internal charge transfer (ICT) at excited states manifested by large Stokes shifts. As ICT excited states are more polar than fundamental states, the Stokes shift increases with the polarity of the solvent. The most common push–pull fluorophores are coumarins [43].
- **Cyanine chromophores** featuring an electron delocalization along a π -conjugated system with an odd number of atoms. They usually possess a thoroughly delocalized charge and small Stokes shifts. The most common cyanine fluorophores are cyanines, squaraines, xanthenes, and bodipy [44].

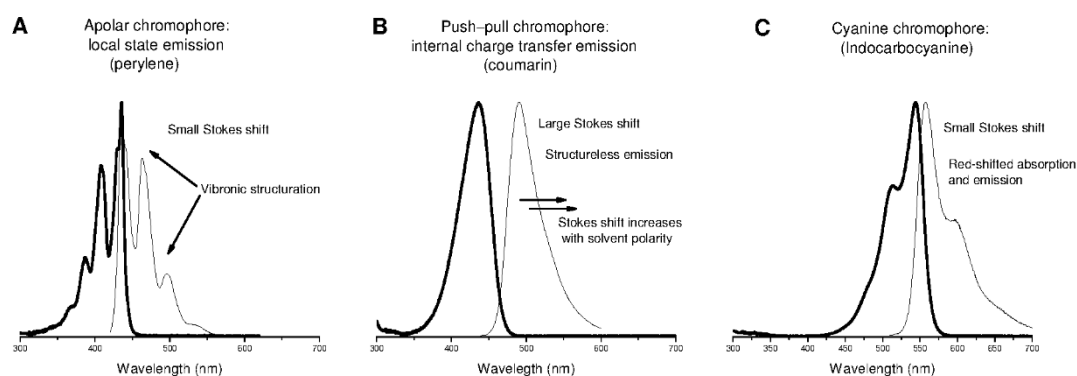


Figure 3. General trend of absorption and emission of three chromophore families. (A) Apolar chromophores; (B) Push–pull chromophores; (C) Cyanine chromophores. (Spectra extracted from photochemCAD) [45].

As fluorescence efficiency and spectral shape are very sensitive to the environment, fluorescence microscopy is an ideal technique to probe and monitor biological environment parameters [46] such as polarity [47,48], viscosity [49–51], hydrophilicity, pH [52], redox potential [53], membrane potential [54,55], and protein mobility (fluorescence recovery after photobleaching (FRAP)) [56] in living cells [57]. The fluorescence properties of a fluorophore can also be impacted by the presence of other chromophores in close vicinity through spatial energy transfers such as FRET (Förster Resonance Energy Transfer) and PET (Photoinduced Electron Transfer) [40–42]. These energy transfer mechanisms have been widely used to design fluorescent bioprobes [58,59].

2.3. Fluorescent Proteins (FPs)

Green fluorescent protein (GFP) from the jellyfish *Aequorea victoria* was discovered in 1962 [60], followed by homologs from diverse marine animals including sea anemone [61], copepod [61], and lancelet [62]. Proteins of the GFP family consist of ~220–240 amino acid residues with 11 β -sheets that form a barrel with a distorted helix inside [2]. At the very center of the β -barrel, 3 amino acid residues of the helix form the chromophore of FPs at positions 65, 66, and 67 (numbering in reference to the GFP of *Aequorea victoria*). A two-step reaction with cyclization of the protein backbone at positions 65–67 followed by dehydrogenation of C α –C β of Tyr66 with molecular oxygen is responsible for the formation of the chromophore. Thus, the chromophore is a two-ring structure representing a conjugated π -system that is large, polarized, and planar enough to absorb and emit light within the visible range [2]. Tyr66 and Gly67 are strictly conserved among natural GFP-like proteins while the residue at position 65 can vary. The side chains of amino acids located inside the barrel play essential roles in chromophore formation and the fine-tuning of spectral properties of cyan, green, and red natural FPs. Variations of these side chains can dramatically alter the excitation and emission spectra [2].

The natural diversity of excitation–emission spectra was further extended via mutagenesis. Today, violet, blue, cyan, green, yellow, orange, red, and far-red monomeric FPs cover almost the whole visible spectrum [2,62–64] (Figure 4). This modern palette is additionally enriched by a number of FP variants (T-Sapphire, mAmetrine, mKeima) with large Stokes shift of more than 100 nm [2]. In addition to monomeric FPs, generation of tandem versions of dimeric FPs (dTomato) [65] or tetrameric FPs (Katushka) [66,67] also exists.

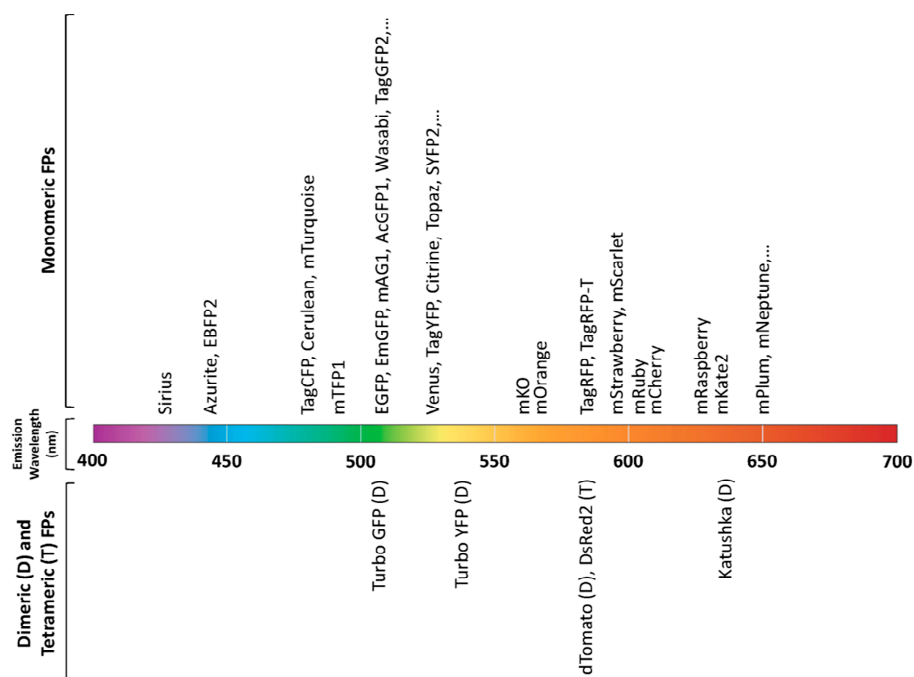


Figure 4. Spectral diversity of selected monomeric, dimeric and tetrameric fluorescent proteins (FPs). FPs are positioned according to their maxima of emission through 1P excitation. Please note that the list of FPs is not exhaustive. Adapted from [2].

FPs are particularly adapted for the development of biosensors used to visualize and quantify various physiological events in living cells, tissues, or whole organisms. There are four main types of biosensors [2,63]:

- **Sensors based on a single FP with no additional protein domain** used for the detection of pH, Cl^- , metal ions, and redox potential variations. Changes of brightness or excitation–emission wavelengths depend on the environment.
- **Sensors built on a single FP fused to conformationally sensitive detector domain(s)** (Ca^{2+} , hydrogen peroxide, phosphorylation, membrane potential). Conformational changes affect spectral properties of the FP.
- **FRET-based sensors** with a change in efficiency of resonance energy transfer between two spectrally differing FPs (Ca^{2+} , cyclic nucleotides, glutamate, kinases, ...).
- **Translocation sensors.** FP fused to specific protein domains demonstrates environmentally dependent changes in intracellular compartments.

In the last decades, advanced fluorescence imaging techniques such as fluorescence lifetime, two-photon microscopy, and nanoscopies have emerged. Using spectroscopic properties of fluorophores, these approaches lead to higher 3D resolution and possibly reduce photodamage to biological samples (see also Section 4).

2.4. Fluorescence Lifetime Imaging Microscopy (FLIM)

Fluorescence lifetime imaging microscopy (FLIM) is an imaging technique which allows mapping of the fluorescence signal as a function of fluorescence lifetime [68–72]. Fluorescence lifetime corresponds to the duration of the existence of a molecule at excited states, in particular at the lowest excited state S_1 . As absorption is considered immediate, the fluorescence lifetime depends mostly on the nature of the Kasha state and de-excitation processes. The fluorescence lifetime is

denoted by τ (Equation (5)) and is expressed as a function of the deactivation kinetics of the excited state (i.e., of the fluorescence rate k_F , intersystem crossing rate k_{ISC} , and internal conversion rate k_{IC}).

$$\tau = \frac{1}{k_F + k_{IC} + k_{ISC}} = \frac{\varphi_F}{k_F} \quad (5)$$

Time-resolved fluorescence measurement provides additional information in comparison with steady-state microscopy as it allows for discriminating several emissions within the same spectral window. The most straightforward time-resolved experiment is the time-gated technique, which involves using a delay between excitation and detection to selectively remove the short-living biological background fluorescence; this technique requires chromophores featuring long-living luminescence, which can be achieved using long-living fluorescence (above 5 ns) [73], phosphorescence [74], lanthanide emission [75], or excimer emission [76]. Time-resolved fluorescence microscopy can be even more selective when using sets of luminophores with very distinctive lifetimes, allowing multiplexing, i.e., separation of several luminescence spectra as functions of fluorescence lifetime [77].

As fluorescence depends both on the nature of the Kasha state and on the competition between several de-excitation processes, fluorescence lifetime is very sensitive to the environment. It allows for measurement of the oxygen concentration [78,79], viscosity [49,80], and pH [81,82].

Fluorescence lifetime imaging can be performed with endogenous (tryptophan, NADH, flavins, porphyrins, melanin, lipofuscin, collagen, etc.) and exogenous fluorophores (small organic fluorophores, FPs, nanoparticles, etc.). Autofluorescence lifetime imaging may provide information on the morphological structure of cells and tissues but the weak and nonspecific fluorescence originating from a variety of endogenous fluorophores limits applications of this method. In contrast, the advantages of exogenous probes are their (i) large structural and spectral diversities, (ii) wide range of fluorescence lifetimes from picoseconds to milliseconds, and (iii) numerous applications in cells, tissues, and whole organs [68]. Notably, due to their organic origin, the majority of small organic fluorophores and FPs have similar characteristics including fluorescence lifetimes within the range of 0.1–4 ns. In addition, both types of molecules share applications in fluorescence lifetime studies including background/autofluorescence elimination and the FLIM-FRET approach [68,83].

2.5. Fluorescent Organic Probes in Two-Photon (2P) Microscopy

2P photon absorption is the simultaneous absorption of two photons to populate an excited state of a chromophore (Figure 5); this is a nonlinear optical phenomenon which depends on the hyperpolarizability of chromophores [84,85]. After excitation, the molecule evolves in a similar way to when exposed to classical excitation, featuring the same fluorescence quantum yield and the same emission spectrum shape. The simultaneous nature of this absorption leads to two main consequences. On one hand, the energy of each photon is half the energy used in one-photon excitation, meaning that the wavelength is doubled in two-photon excitation compared to in classical excitation. As a matter of fact, excitation of fluorochromes and collection of photons within the biological transparency windows are much easier and lead to deeper tissue penetration and less photodamage to living cells (Figure 5).

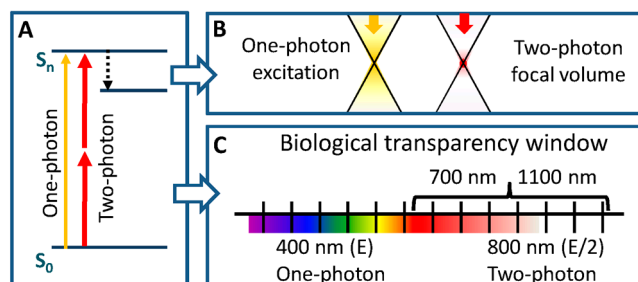


Figure 5. Principle of two-photon absorption. (A) Simultaneous two-photon absorption; (B) Comparison of excitation volume in one- versus two-photon absorption; (C) Two-photon absorption allows shifting the excitation of UV–visible fluorophores in the near-infrared region within the biological transparency window. The energy of each photon in two-photon absorption is halved ($E/2$) in comparison with that in classical absorption (E).

On the other hand, the simultaneity of photon absorption implies a nonlinear probability for photon absorption, which depends on the square of incident light intensity. The square dependence allows us to better restrict the excitation to a focal volume that determines a better control of the excitation depth [86,87]. Two-photon absorbing molecules have been developed [88,89] allowing images of deeper inside a tissue ($>100\ \mu\text{m}$) to be obtained with higher spatial resolution and longer observation time. Although many “one-photon” dyes can also be excited under two-photon irradiation conditions, their structure is not optimized for this technique as they have a small two-photon absorption cross section. The particular design of two-photon probes has been well rationalized by theoretical approaches [85]. It was shown that electron delocalization plays the main role in two-photon absorption. Indeed, privileged chromophores for two-photon absorption are highly polarizable molecules featuring strong internal charge transfer upon irradiation (Figure 6). They feature both long conjugation systems and strong electron donating and withdrawing groups to create the strongest electron delocalization. Chromophore geometry may also play a determining role. In particular, quadrupolar, octupolar, or cyanine structures increase 2P absorption thanks to resonances with low energy states (Figure 6) [85,90].

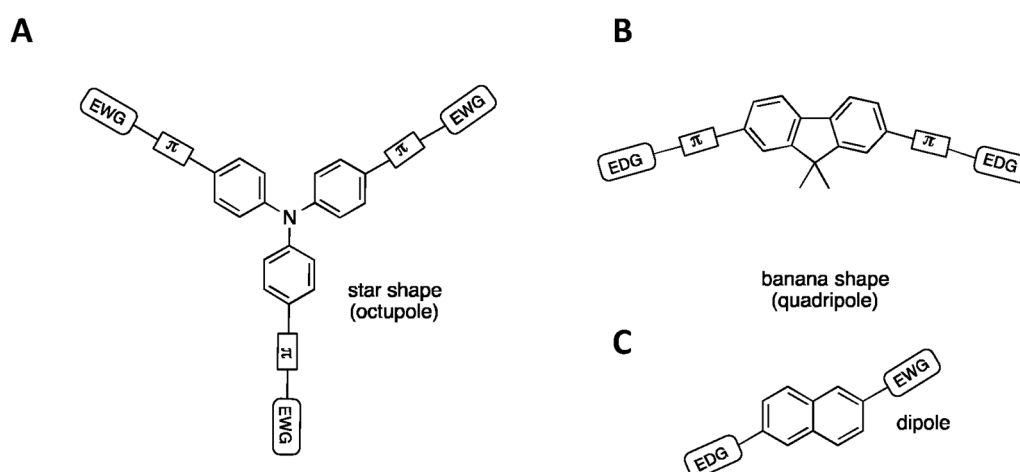


Figure 6. Preferred structures for two-photon absorption. (A) Star shape or octupole; (B) Banana shape or quadrupole; (C) Dipole. EWG, Electron-Withdrawing Group; EDG, Electron-Donating Group; π , conjugated π system.

In addition to these synthetic small organic molecules, FPs are also suitable for 2P absorption. However, the 2P optimum excitation wavelength and maximum brightness of FPs cannot, in general, be deduced from 1P properties because (i) the chromophore of FPs is not centrosymmetric and (ii) there is an enhancement of certain vibronic transitions in the 2P absorption spectrum of FPs [91].

Compared with a small fluorescent organic molecule in solution, the chromophore of FPs is buried within a complex protein environment that influences the photophysical properties of the chromophore through electrostatic interactions. In particular, the internal electric field inside the β -barrel influences the 2P properties of FPs, including the cross section [91,92]. Recently, blue-shifted green fluorescent protein homologs have been shown to be 2.5 times brighter than the commonly used enhanced GFP under 2P excitation [92].

2.6. Fluorescent Organic Probes in Nanoscopy

A general restriction of fluorescence imaging is the Abbe light diffraction limit. Very simply, if the distance between two emitting fluorophores is shorter than half the wavelength used, it is impossible to isolate the emission of each molecule, making the image blurred. To bypass this limit, super-resolution fluorescence imaging techniques were implemented to individually isolate the emission of each fluorophore. These techniques are generally classified into two main categories: fluorescence depletion and stochastic approaches [6,93]. STimulated Emission Depletion (STED) nanoscopy is the most widespread fluorescence depletion technique, and uses stimulated emission to prevent the spontaneous emission of fluorescence in the vicinity of target fluorophores. Practically, STED relies on two distinct excitations: a diffraction-limited classical excitation followed by a structured toroidal excitation, which depopulates the excited state of fluorophores by stimulated emission at the periphery of the first excitation circle. Consequently, depopulation allows for retaining only the fluorescence of fluorophores at the very center of the irradiation (Figure 7) [94–96].

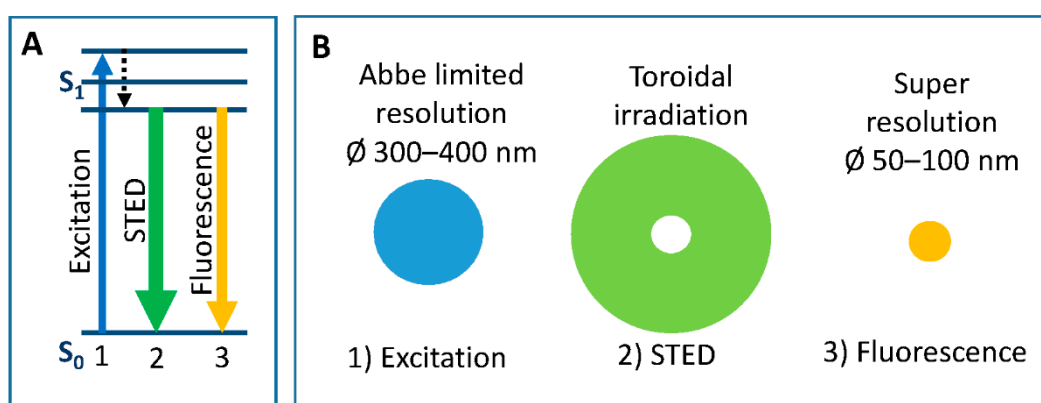


Figure 7. Sequences for STimulated Emission Depletion (STED) nanoscopy. (A) Energy diagram; (B) Spatial distribution. (1) Excitation, (2) deactivation of peripheral fluorophores by toroidal STED irradiation, and (3) fluorescence of fluorophores localized at the center of the excitation spot.

The other family of nanoscopy methods is the stochastic approach in which fluorophores are initially in a dark state (nonfluorescent state) (Figure 8). Few spatially separated molecules are then activated, localized by the emitted fluorescence, and then deactivated. Several cycles of activation/deactivation are used to map the biological sample (Figure 8). The fluorescence switching process can be induced in several ways. The first strategy is called Photo-Activated Localization Microscopy (PALM) and may use “dark-state” fluorophores requiring irradiation to become fluorescent [97,98]. After fluorescence signal detection, fluorophores are photobleached under irradiation and other “dark-state” fluorophores are activated. In a second method, named Binding Activated Localization Microscopy or Points Accumulation for Imaging in Nanoscale Topography (BALM/PAINT), dark-state fluorophores are briefly activated only during interaction with a specific substrate [99]. An alternative to the PALM technique is the STochastic Optical Reconstruction Microscopy (STORM) using photoswitchable dyes whose fluorescence can be triggered or inhibited by light irradiation [100–102].

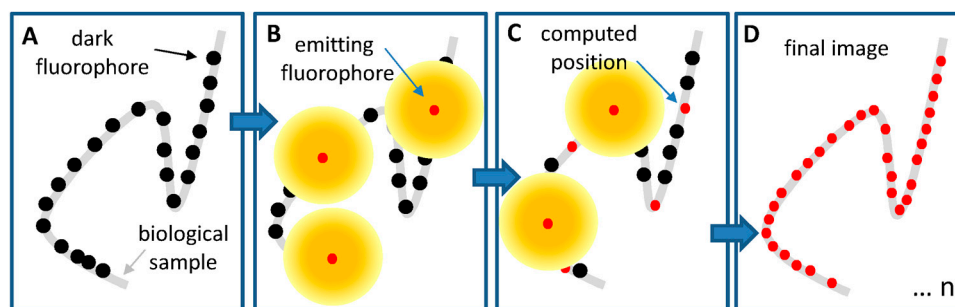


Figure 8. Sequences for stochastic imaging. (A) Fluorophores initially in a dark state grafted onto a biological sample; (B) Some well-separated fluorophores are activated and their emission (yellow circles) allows for localizing them (red points); (C) Deactivation and activation of other fluorophores; (D) After n iterations, the final image is created corresponding to the geometry of the biological sample.

Recent developments of small fluorescent organic probes for nanoscopies will be discussed in Section 4.2. For FPs, new variants of so-called photocontrollable FPs have been engineered, notably for nanoscopies, and can be classified into three forms [103,104]:

- **Photoactivatable FPs (PAFPs)** which undergo activation from a nonfluorescent (dark) state to a fluorescent state (PAMTagRFP, PAMKate, ...).
- **Photoswitchable (also called photoconvertible) FPs (PSFPs)** that can be converted from one fluorescent state to another (Dendra2, mEos2, ...).
- **Reversibly photoswitchable FPs (rsFPs).** rsFPs can be photoswitched repeatedly between fluorescent and nonfluorescent states (rsEGFP, rsTagRFP, ...).

3. Strategies for Labeling Living Samples with Fluorescent Probes

In addition to their photophysical properties, fluorescent organic probes should have essential physicochemical properties for easy use with living samples. The membrane permeability of small organic fluorophores depends on their lipophilicity, their molecular weight, the number of hydrogen bond donors/acceptors, and their charge [105]. Therefore, cell-permeant probes are preferred but cell loading could also be achieved by other techniques that involve iontophoresis, ejection of a substance from a pipette by the application of current, or pressure injection using intracellular micropipettes [106]. Once inside the cell, probes should be well-retained within the cell or, in some cases, need the support of multidrug resistance protein family inhibitors to reduce extrusion [107]. The sensitivity and specificity of the small fluorescent organic probe determine the use concentration and consequently limit cytotoxicity or physiological modifications. For FPs, the expression level of a fusion construct (protein of interest–FP) should be good enough to obtain a sufficient signal for reliable imaging and not too high in order to avoid interfering with the biochemistry of a living cell. In transient transfection (introduction of fusion-construct-containing plasmid in cells), the expression level may vary among transfected cells. For robust and reproducible experiments, stable cell lines (integration of the transfected plasmid into the target cell genome) are preferred [2]. Finally, photostability of the fluorescent organic probe is directly responsible for the duration of the experiment and the frequency of image acquisition.

The aim of this section is not to propose a comprehensive and extensive catalog but rather to underline through mostly, but not exclusively, in situ examples the required characteristics of fluorescent organic probes with regard to applications and type of living samples (Table 1). Thanks to their easy access, isolated cells offer the greatest possibilities for cellular and intracellular labeling and they will be firstly described. Although most labeling methods for isolated cells may be applicable to other type of samples, adaptation or complementary strategies have also been developed to reach similar targets in tissues, organs, and organisms.

3.1. Strategies of Labeling for Isolated Living Cells

3.1.1. Fluorescent Labeling to Monitor Cell Viability

Monitoring cell viability is one of the earlier applications of fluorescent probes and is mainly based on plasma membrane integrity (Table 1). To facilitate membrane permeation, probes such as fluorescein diacetate (FDA) or calcein have been designed with an organic complex acetoxymethylester group (AM, R: $-\text{CH}_2\text{OCOCH}_3$) [108]. Outside the cell, the probe is not fluorescent and penetrates the cell membrane thanks to the AM group, which is then cleaved by endogenous esterases [109]. Once the AM is removed, the probe is strongly fluorescent and trapped within the cell, although leakage can be observed over time. FDA is a low-cost and easy-to-use probe, but is, unfortunately, poorly retained in cells. Consequently, cells are often lysed before fluorescence measurement through plate readers to obtain the full signal [110,111]. Calcein is also frequently used for cell viability purposes but has the drawback of being sensitive to light exposure, and rapid photobleaching may limit experimental duration. To refine the experimental procedure by monitoring the ratio of living and dead cells, calcein is usually combined with a cell-impermeant DNA-intercalating agent such as propidium iodide or ethidium bromide that reaches their target only in cells with fragmented plasma membranes. More recently, a new generation of ready-to-use reagents (Nuc family) for dead or live cells has emerged which exhibits a very low basal fluorescence and emits a very bright fluorescence signal when bound to DNA [112,113].

3.1.2. Fluorescent Labeling for Cell Tracking

Cell tracking is associated with short and long time lapses for which the ability of the probe to be retained in the cell is an essential criterion (Table 1). Due to reactivity with the thiol group of cellular macromolecules, FDA-derived probes commercially known as the Cell Tracker family are frequently used to perform short time lapses [114]. Cell trackers label the entire cytoplasm but cell loading might depend on the cell type or cell metabolism. To reduce photocytotoxicity induced by repetitive light exposure, near-red probes such as Red or Deep Red CytoTracker are preferred because they are excited with low-energy radiation (see also Section 2.5). Lipophilic tracers including long-chain dialkylcarbocyanines such as 1,1'-dioctadecyl-3,3,3',3'-tetramethylindocarbocyanine perchlorate (DiI) or the CellVue family finely and intensively stain membrane structures [115,116] and could represent convenient markers for long-term tracking. Alternatively, a new technology has been recently developed to stably incorporate a red fluorescent dye containing hydrophobic aliphatic chains into the lipids of plasma membrane [117]. Note that nonorganic probes such as Quantum Dots may also be used for cell tracking but will not be detailed here.

3.1.3. Fluorescent Labeling to Identify Membrane, Organelles, and Macromolecules

Indirect staining of membranous elements by using lectins that reversibly bind to glycoproteins, glycolipids, or polysaccharides is a very simple and convenient strategy (Table 1) [118]. In particular, wheat germ agglutinin (WGA) is a protein that recognizes *N*-acetylglucosamine and *N*-acetylneuraminic acid residue present at the cell surface of numerous eukaryotes and prokaryotes [119]. A broad range of fluorescent Alexa-WGA conjugates is commercially available but their labeling intensity and photostability are associated with photophysical characteristics of the fluorochrome [120,121]. Therefore, short-term incubation with fluorescent WGA conjugates induces a bright cellular outline including processes and intercellular connections [114,122]. Due to membrane internalization and vesicle recycling processes, fluorescent lectins can also be detected and followed in intracellular compartments or elements over time [122]. Nevertheless, considering the large distribution of the target residues, WGA could not be considered a discriminating marker.

Nuclear, mitochondrial, and cytosolic nucleic acids could be labeled in living cells with rarer cell-permeant probes (Table 1). Historically, the Hoechst intercalant DNA family was used but it has spectral drawbacks with a high-energy UV peak of excitation that is phototoxic to cells and a

broad emission, a source of spectral contamination during multilabeling experiments [123]. However, Hoechst dyes are now conjugated to various molecules to tether them to DNA [124]. More recently, a new generation of cyanine probes called the SYTO[®] family offers a large diversity of both ex/em wavelength couples and DNA/RNA affinities. Consequently, cellular localization of the nucleus in the case of counter-staining and multiplex fluorescent signals and/or specific nucleic acid detection are now facilitated by the use of SYTO[®] probes [113].

Labeling and tracking organelles in living cells is not a trivial issue (Table 1). As a striking example, localization of actively respiring mitochondria with organic dyes needs particular attention. Containing a thiol-reactive chloromethyl moiety, dyes from the “Mitotracker” family are widely used nowadays to follow mitochondria within a cell or from cell to cell [125]. Mitochondria have been shown to display the capacity to be transferred between cell types, notably in the context of cancer [126]. Co-culture experiments with a combination of Mitotracker and vital dye have been recently performed and clearly identify the transfer of mitochondria from donor cells to target cells [127]. Although there is a broad variety of fluorescent Mitotrackers, differential signal intensity and differential distribution may be noted between them. In particular, localization of mitochondria is different with Mitotracker Green FM compared with Mitotracker Red CMXRos in PC12 cells (Figure 9) and more cell leakage is observed for Mitotracker Red. On the contrary, there is potentially more cytotoxicity with Mitotracker Green labeling during long time lapses as we observed through videomicroscopy. As previously mentioned, the aim of this section is not to propose a catalog of fluorescent probes for living cells but to note that there are numerous dyes or strategies to label other organelles including lysosomes, peroxisomes, endosomes, endoplasmic reticulum, or Golgi apparatus. Among these strategies, the BacMam method with insect baculovirus (CellLight[®]), available for most organelles, leads to the introduction of a fluorescent protein which is a specific marker of the organelle [33]. For lysosomes, probes such as Lyso trackers or Lyso sensors take advantage of the acidity/pH of these organelles for fluorescent labeling [128]. More recently, new organic fluorescent probes with high photostability have been developed to follow lysosome (peptide-based and Atto) and mitochondrion (NHS ester and Atto) dynamics and interaction during super-resolution time-lapse experiments [129].

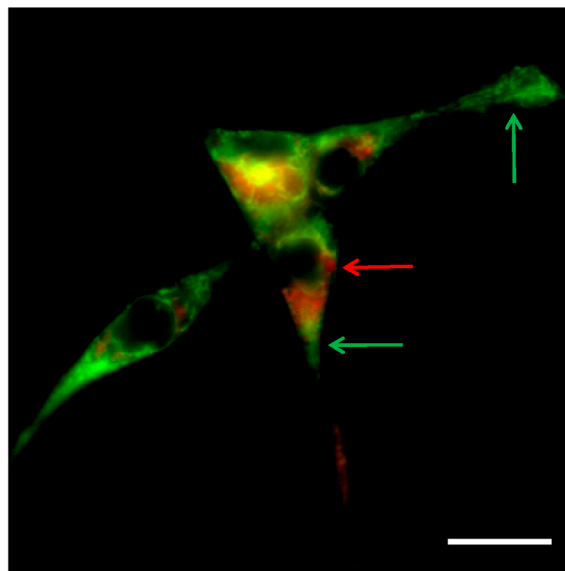


Figure 9. Comparative distribution of mitochondria labeled with Mitotracker Green FM (MTG) and/or Mitotracker Red CMXRos (MTR) in living PC12 cells. PC12 cells were incubated simultaneously for 30 min at 37 °C with 10 μ M of MTG and 10 μ M of MTR. Overlay shows MTG staining in green and MTR in red color through wide-field microscopy imaging (X63 oil immersion objective). Green and red arrows indicate mitochondria exclusively labeled with MTG or MTR respectively. Scale bar: 20 μ m.

To reduce light-induced cellular stress, a new family of near-infrared or infrared fluorophores named silicon rhodamine probes (SiR probes) has been recently developed for DNA, cytoskeleton protein, and lysosome detection (Table 1) (see also Section 4.1 for chemical structure and advantages) [130]. Depending on the cell type, SiR probes might be excluded and, consequently, cell loading could be weak. Therefore, concomitant incubation with verapamil, a broad-spectrum efflux pump inhibitor, may improve fluorescent staining with SiR probes [131]. An alternative strategy to obtain an intense and long-term fluorescent signal is to infect cells with lentivectors known as Cyto-Tracers™ that expressed fluorochrome-fusion tracer proteins [132]. Therefore, these vectors produce fluorescent proteins that are specifically integrated into organelles or cellular targets and used for tracer dynamic studies [132].

To visualize glycan and lipids in cells for which, in contrast to proteins, genetically encoded reporters are not possible, click chemistry has been recently adapted to overcome the lack of methods (Table 1) [133]. The principle of click chemistry consists of cultivating cells in the presence of non-natural metabolite derivatives that carry “clickable” functions such as azide or alkyne groups (Figure 10A). These derivatives must cross the cell membrane and be accepted by the biosynthetic machinery of the cell [134]. Once metabolized and presented on the cell surface, the azide (or alkyne)-containing molecule can be visualized through a bioorthogonal ligation reaction with a fluorescent reporter using cuprous Cu(I) ions as catalyst (Figure 10). Numerous derivatives have been synthesized to date and been used to label various molecules in animal cells, bacteria, yeast, and plant cells, and they are now widely used for glycobiology, especially to study the function of carbohydrates or glycomolecules in living systems. For example, lipopolysaccharides of Gram-negative bacteria can be labeled using an azide-modified analogue of 3-deoxy-D-manno-octulosonic acid (Kdo-N3) [135] and glycans were recently visualized with *N*-azidoacetylmannosamine in HEK293T cells [134]. The azide group is exploited for because it possesses a high reactivity, is stable in water, unreactive in biological samples, and does not perturb the structural conformation of the modified molecule. The prototypical click reaction termed as azide–alkyne cycloaddition (Figure 10A) is one of the three main click reactions used for molecule labeling. In fact, two other reactions—the copper-free azide–alkyne cycloaddition between an azide group and a strained cyclooctyne and the Staudinger ligation between an azide group and a phosphine—are also commonly employed for labeling of biological molecules. These two last reactions are of major interest because they do not need to be catalyzed by copper and are thus effective for *in vivo* labeling. While these reactions are of main interest as they exhibit strong selectivity, the choice of reaction when initiating studies is of main importance as side effects such as copper toxicity, changes in membrane permeability, and unspecific or background labeling can be problematic. For example, alkynyl sugars worked better than the azide form for labeling in mouse [136], probably because azide sugars could be toxic at high concentrations. However, azide sugars showed no toxicity in plant cells [137]. Moreover, the alkynyl fluorophore is also generally more efficient than the azide form but can lead to unspecific or high background labeling. Thus, the choice of the alkynyl–azide couple is of main importance when choosing click chemistry for labeling.

Cellular localization and co-localization of molecules of interest require both cytological references (membrane, nucleus, etc.), also called counter-staining, and multiplex fluorescent signals. Consequently, it is necessary to activate as many excitation wavelengths as fluorescent probes. However, special attention has to be paid on spectral overlapping of emitting light to avoid any artifactual detection of fluorescence, i.e., detection of emitted light by fluorochrome #1 in channel detection of fluorochrome #2. In addition, autofluorescence may be present in samples such as plants [138] and microalgae [139] and its spectral characterization through $\lambda\lambda$ scan (excitation/emission) is essential to choosing the appropriate fluorescent probe(s). Multilabeling experiments also suggest that a sequential mode of acquisition (one by one) may increase the duration of acquisition and the duration of light exposure, leading consequently to phototoxicity and photobleaching (see also Section 5).

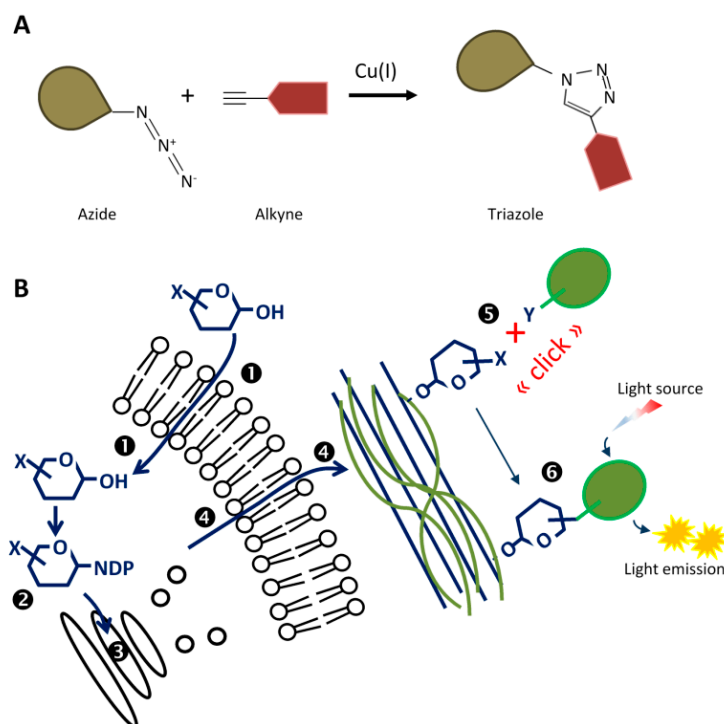


Figure 10. Principle of bioorthogonal reaction. (A) Bioorthogonal reaction of the azide–alkyne cycloaddition, also termed as a “click reaction”, in the presence of cuprous $Cu(I)$ ions. (B) Schematic representation of the incorporation of a clickable sugar (X-sugar) ①, its activation as a nucleotide sugar (NDP sugar) ②, metabolic modification ③, excretion ④, labeling after click reaction with a compatible fluorophore (Y-fluorophore) ⑤ and its visualization under light excitation ⑥. NDP: nucleotide diphosphate (mostly UridineDP or GuanineDP). X-sugar-NDP is an “activated glycosyl donor” which is the substrate of glycosyltransferases.

3.1.4. Fluorescent Labeling to Monitor Cellular Activities

- Protein Function

One of the most common ways to study the functional role of a protein is to incorporate in a cell a vector with genetic material tagged with a fluorescence sequence (Table 1). Besides the impact of the fluorescent tag size on the function of the protein of interest, many transfection strategies are used and have to be considered regarding their efficiency and their cytotoxicity. Lipofectant agents (transient pores in the cell membrane induced by calcium phosphate, cationic lipids, etc.) or electroporation (or electroporomeabilization; increase in cell membrane permeability induced by an electrical field) are two main methods used to induce penetration of a plasmid into targeted cells. As one example, GFP-chromogranin A (CgA-GFP) is expressed in living COS-7 cells after transfection with lipofectamine and allows the tracking of secretory granules during granulogenesis [140]. More recently, a liposomal carrier system has been developed and offers a high yield of transfection combined with very low toxicity in mammalian cells [141]. Targeted introduction of a DNA sequence could also be performed with a modified insect cell baculovirus that infects and expresses genes in mammalian cells [113]. However, depending on the cell type, cytotoxicity and a poor yield of infection can be observed. Alternatively, new types of fusion protein–tag platforms including tetracysteine tag [142], SNAP/CLIP-tag [143,144], and HaloTag [145] have emerged more recently [146]. In these methods, the tag can be conveniently labeled with small organic fluorophores added to the incubation medium of living cells. For the tetracysteine system, a short peptide sequence (6 to 12 amino acid binding motifs) is genetically introduced into the sequence of a target protein. This sequence can specifically react with cell-permeant biarsenical fluorophores (FIAsH-EDT2 and ReASH) [147]. Similar in size to FPs, SNAP/CLIP-tag and HaloTag are self-labeling enzymes. SNAP and CLIP, variants of the

human O⁶-alkylguanine-DNA alkyltransferase (AGT), are used to visualize cellular proteins with fluorescent O⁶-benzylguanine and O²-benzylcytosine substrates, respectively [144]. In particular, single-molecule imaging of SNAP-tagged fusion proteins has been developed with Dy 549 and CF 640 coupled benzylguanines [148]. HaloTag is a modified bacterial hydrolase enzyme designed to fuse to a protein of interest and to facilitate visualization of its subcellular localization. This HaloTag technology is based on the formation of a specific and irreversible covalent bond (chloroalkane linker) between the HaloTag protein fusion and synthetic ligands that carry a variety of functionalities including a fluorescent group for in vitro cellular imaging (TMR, diAcFAM, Oregon Green, Coumarin, or Alexa Fluor 488) [149].

- Cell Metabolism

Due to their high sensitivity and fast response time, small-molecule-based nonratiometric/ratiometric fluorescence sensor systems for monitoring cell activity variations are widely used nowadays [58]. The binding affinity of the probe for its target is characterized by the dissociation constant (K_D), expressed in nM, that may also be dependent on pH and ionic strength [128]. Nonratiometric probes do not emit fluorescence (or emit low fluorescence) in the absence of the target molecule while ratiometric ones exhibit differential light emission/absorption whether they are coupled or not to the analyte [128]. When quantification is required, ratiometric organic probes are usually used to limit interference from the subcellular microenvironment, instrumental parameters, local concentration of the probe, and photobleaching, and to therefore provide effective internal referencing [58]. Related to their design, four classes of ratiometric probes have been identified so far including internal charge transfer (ICT; cation sensing), excited-state intramolecular proton transfer (ESIPT; fluoride, acetate, metal ion sensing), fluorescence resonance energy transfer (FRET; metal cation sensing) and through-bond energy transfer (TBET; metal cation sensing), and monomer–excimer formation (metal ions, phosphate, nucleic acid sensing) [58]. However, the use of ratiometric probes has a direct impact on the choice of instrument since efficient simultaneous detection or excitation is mandatory. Note that cell loading could be facilitated by dispersing agents that will increase the bioavailability of the probe [150]. There are a number of ratiometric Ca²⁺ ion indicators including Fura-2 and Indo-1 AM [151,152]. For simplicity of use, notably for Ca²⁺ studies on cell populations using plate readers or confocal microscopes, the nonratiometric probe Fluo-4 AM might be preferred [153,154]. For plant samples such as pollen tubes and root hairs, a cell lysis solution is needed to improve Fluo-4 AM loading [155]. Many ratiometric and nonratiometric indicators for sodium (CoroNa, SBFI) [156], zinc (FluoZin-1, FluoZin-3) [157], and magnesium (Mag-Fura-2, Magnesium Green, KMG-20-AM, and KMG-27-AM) [158] are also available. JC-1 (tetraethylbenzimidazolylcarbocyanine iodide) revealed mitochondrial activity through ratiometric monitoring of membrane potential. When mitochondrial membrane potential is high, suggesting healthy hyperpolarized mitochondria, the dye form aggregates and emits a red fluorescence with a maximum peak at 590 nm. When mitochondrial membrane potential is low (depolarization), JC-1 has predominantly a monomer form and emits green fluorescence with a peak of emission at 530 nm [159]. Cell metabolism is also followed by monitoring cellular stress revealed by organic probes (H2DCFDA, Luminol, RedocSensor, MTT) for reactive oxygen species (ROS) detection [160,161], boronobenzo[b]quinolizinium derivatives for H₂O₂ [162], Si-rhodamine deoxylactam-based near-infrared fluorescent probe for nitric oxide (NO) [163], or by determining apoptosis with fluorescent marker fluorescein isothiocyanate carbobenzoxy-valyl-alanyl-aspartyl-[O-methyl]-fluoromethylketone (FITC-VAD-FMK) for the detection of caspase activity [110]. The combination of a cell-permeant fluorescent polymer thermometer called NN-AP2.5, which notably consists of a thermosensitive poly(*N*-*n*-propylacrylamide) unit, with FLIM leads to intracellular temperature monitoring between 28 °C and 38 °C in HeLa cells [164].

Consequently, there is a huge range of small fluorescent organic molecules available for cell metabolism studies and the choice of probe should be driven by their selectivity and specificity

described in the literature and technical notes. Cellular environment considerations may also increase the difficulty of the choice since intracellular factors including pH, concentration of competing metals, ionic strength, preference for hydrophobic regions, and binding constants influence specificity and sensitivity of fluorescent dyes. In particular, fluorescence generated by Zn^{2+} and Ca^{2+} probes within cells may also result from nonselective binding to labile and protein-bound as well as membrane-bound metals and/or from nonspecific affinity for other divalent cations [165].

An alternative to organic probes for detection of cell activity is the recent development of a number of biosensors with numerous genetic constructions mostly related to the GFP protein family [166] (Table 1). This approach includes a vector transfection step of genetically encoded FRET biosensor(s) [167]. Biosensor expression offers many possibilities to study molecular mechanisms in living cells including calcium, PKA, and ERK activities through FLIM-FRET experiments [168,169]. With the development of lifetime imaging systems and new fluorescent proteins, simultaneous use of two FLIM-FRET biosensors within one sample is allowed [169,170]. The biosensor strategy may bypass difficulties like probe penetration and autofluorescence in plants or microalgae [171]. In addition, photoactivation-induced specific expression of biosensors in a group of cells, in cells, and in subcellular compartments offers a new perspective in cell biology studies [172]. In the context of oocyte development, photoactivation of a subpopulation of microtubule subunits contributed to understanding of the comprehensive dynamics of microtubules within the mouse egg spindle [173].

3.2. Strategies of Labeling Living Cells within Organotypic Slices or Organs

Living organs and cultured organotypic slices offer the possibility to study cell responses within a microenvironment in which connections between cells and interactions with the extracellular matrix or vascular networks are preserved. Consequently, direct access to probes is sometimes limited and cell labeling may be more difficult (Table 1). While extended time of incubation could be sufficient for some cell-permeant fluorescent probes, others cannot be used. In particular, a high level of plasma and extracellular esterase activity render the classical acetoxymethyl (AM) probes ineffective for monitoring intracellular events *ex vivo* or *in vivo* [108]. Because widefield microscopes do not have any way to eliminate out-of-focus light, samples thicker than 10–20 μm may have dramatically reduced image quality. Consequently, confocal micro- and macroscopy, equipped with a pinhole in the detection path, as well as 2P microscopy whose excitation is restricted to the tiny focal volume, are preferred over wide-field microscopy for thicker samples. Live- or dead-cell fluorescent markers probes such as Syto 61, Sytox Orange, TO-PRO-3, or YO-PRO-1 may be used for cell viability or counterstaining [174,175]. However, cell metabolism indicators such as ROS would give more informative data on the real state of the sample rather than a simple calcein labeling [176]. As a nonratiometric Ca^{2+} sensor, Oregon Green 488 BAPTA-1, which presents a high absorptivity (~93%), is more efficiently excited by a 488 nm laser line than are other Ca^{2+} dyes (~45% of maximum absorptivity for fluo-3 and calcium green indicators) [128]. Consequently, less laser power is necessary to measure calcium variations in brain slices, reducing phototoxicity and photobleaching [177,178]. More recently, variations of Ca^{2+} concentrations have been monitored with a calcium biosensor (TN L15) through FLIM-FRET experiments in neurons of hippocampal slices [179]. In contrast, cell markers previously described for isolated cells such as CMFDA or DiI have been successively used in several types of samples including cerebellar slices to study neuronal migration during development [111,177,180]. Both probes exhibit intense fluorescence signals and photostability since time lapses of up to 12 h have been performed with dry, long working distance objective (for more details see also Section 5.2) through confocal macroscopy [111]. Fluorescent lectins such as IB4 derived from *Griffonia simplicifolia* seeds also penetrate tissues efficiently. As one example, IB4 selectively stains parenchymal microglia and endothelial cells and thus provides a simple one-step method to label brain slices [175]. Another strategy is to use a virus such as the herpes simplex virus (HSV) that will infect targeted cell types under the control of specific gene promoter. Infected cells will consequently express fluorescent proteins including biosensors in brain slices [180,181]. Alternative to transfer techniques such as microinjection, biolistic

gene gun, viral infection, lipofection, and transgenic technology that are not suitable for gene transfer into a single cell or a small number of cells, a method with local application of plasmid solution and a small current injection (electroporation) was developed to study axon morphology of individual cortical neurons in organotypic slice cultures [182]. To label organ vascular pathways, one possibility is to inject tracers directly in the blood or lymphatic circulation of living organisms. Ligating is then necessary to remove the organ and to reduce leakage from the vessels as it was performed for ex vivo observation of rat heart labeled with FITC-dextran through confocal macroscopy (Figure 11) [183].

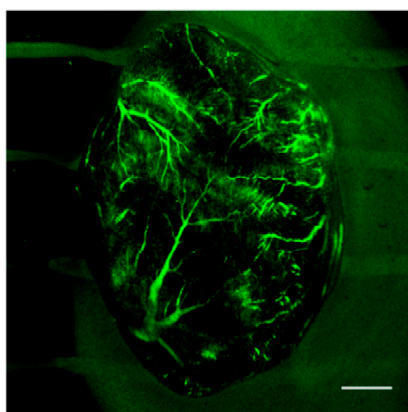


Figure 11. Ex vivo cartography of cardiac blood vasculature. Intravenous injection of fluorescein isothiocyanate (FITC)-dextran was performed in anaesthetized animals (for experimental procedures, please see [183]). After ligating, the heart was removed and directly placed on the stage of a confocal macroscope for imaging. FITC-dextran labeled blood circulation. Scale bar: 1 mm.

3.3. Strategies for Labeling Living Cells within an Organism

The strategy of labeling, together with the strategy of access for imaging, should be adapted to the type of organism (unicellular organisms, larvae, embryos, pups, plants, insects, adult rodents, etc.) and possibly to the type of target organ within the organism (Table 1). Some strategies will require anesthesia and invasive methods such as surgery (skin sectioning, laparotomy, cranial window, etc.) to access to the area of interest (muscle, embryos, intestine, heart, brain, etc.). Other strategies of labeling and observation are noninvasive, but they may need anesthesia and are limited to organism restraint or immobilization and hair shaving. In addition, spectral characteristics of the probe might be driven by the thickness and the transparency of tissues. As a general principle, the use of long wavelengths, as for near-infrared or infrared probes, results in reduced scatter losses and, consequently, increased tissue penetration and deeper imaging. As an example, a new cyanine-based NIR fluorescent probe was recently developed for the detection of Zn^{2+} in zebrafish [184]. Regarding the instruments, confocal macroscopy, fibered confocal microscopy, two-photon microscopy, and light sheet fluorescence microscopy (LSFM) are technologies of choice for imaging organisms. In LSFM, a thin excitation light sheet illuminates a single plane of the specimen via an illumination objective. The emitted fluorescence signals are detected by a second objective which is mounted perpendicular to the illumination axis. A specimen holder is automatically moved to obtain images, plane by plane, throughout the whole sample, and resulting image stacks are used for 3D reconstruction [36]. Therefore, large field of view, rapid acquisition with detectors such as Electron-Multiplication CCD cameras (EM-CCD) and scientific Complementary Metal Oxide Semiconductor (sCMOS) cameras (see also Section 5.3), good signal-to-noise ratio (SNR), and undamaged sample above or below the focal plane are LSFM features particularly adapted to studying living transparent specimens such as growing plants, drosophila larvae, and zebrafish [36,185].

3.3.1. Injection of Fluorescent Probes and Labeled Cells

As described in Section 3.2, fluorescent probes can be injected through the vascular pathway and systemic circulation to reach organs in organisms. After surgery, the probe can also be injected directly within the organ or organism (Table 1). To trace the neural circuit, Levy et al. [186] injected Alexa 488-WGA lectin directly within the mouse cerebellum. Injection of DiI/3,3'-diiododipropylcarbocyanine perchlorate, DiO, in the mesenchym of chick embryo offers the possibility to follow dynamics of tissue deformation during hindlimb development [187]. More simply, organs can only be bathed in a solution of fluorescent probes for several minutes. Observation through intravital microscopy of exposed submandibular gland acini incubated with Mitotracker revealed synchronization of mitochondrial metabolic oscillations [188]. In xenograft protocols, cells could be labeled before injection in an organism and consequently be easily imaged or even tracked later on. Injection of SiR700-labeled antibody-containing HKBMM cells in mouse induces a tumor that can consequently be detected through in vivo imaging [189].

3.3.2. Transfection through Electroporation and Transgenic Organisms

There are two approaches to labeling organisms with fluorescent proteins (Table 1). The first one consists of injecting a plasmid expressing a tagged protein into an organism followed by electroporation to allow the vector to penetrate targeted cells. Microinjection of a GFP-tagged plasmid into the lateral ventricle of the embryonic rat brain (E15.5 or E18.5) followed by electroporation (5 electric pulses, 50 V, 50 ms) revealed p57(Kip2) effects on neurogenesis and gliogenesis [190]. The second approach is to obtain through genetic engineering transgenic organisms with total or targeted expression of proteins or biosensors [191].

3.3.3. Click Chemistry in Living Organisms

The principle of click chemistry developed in cultured cells has been recently applied to living organisms to accumulate small molecules at a potential site of injury (Table 1). As an illustration of in vivo application, Tetrazine (Tz) or Azide (Az) alginate gels were firstly injected intramuscularly or into the mouse mammary fat pad [192]. Then, intravenous injections of Cy5-*trans*-cyclooctene (TCO) or Cy7-dibenzocyclooctyne (DBCO) induced respective fluorescence emission in Tz and Az gels, revealing click chemistry reactions [192]. In addition to azide-alkyne cycloadditions, thiol-ene click reactions are also widely used to form hydrogels—delivery vehicles of cells and therapeutics including small-molecule drugs, peptides, or proteins [193]. Reactions of thiol-containing macromolecules (polyethylene glycol, etc.) with alkenes (vinyl sulfone, maleimides, norbornene, etc.) may occur in situ [194] and time release of fluorescent cargo molecules (albumin, IgG, etc.) is notably dependent on thiol composition [195]. These data suggest new perspectives for click chemistry in disease treatment including controlled drug delivery.

In plant glycobiology, click chemistry represents a very powerful tool to study the cell wall—the complex matrix made of carbohydrate and proteins which ensures the mechanical integrity of plant tissue but also permits cell expansion after physical and enzymatic modification and determines cell shape [196] (Figure 10B).

To date, click labeling of plant cell wall has been used to study pectic polysaccharides [135] (Figure 12A), an unknown wall component in root hair tips [197], and monolignol in secondary cell wall [198,199]. These studies showed that fucose alkyne is successfully incorporated, metabolized, and labeled in plant cell wall pectic polysaccharide Rhamnogalacturonan I [200] (Figure 12(A2)). Moreover, the labeling of rhamnogalacturonane II (RG-II) with Kdo-N3 (Figure 12(A1)) demonstrated that incorporation of Kdo-N3 occurs in RG-II, a highly complex pectic component, through the endogenous biosynthetic machinery of the cell, and co-localization with calcofluor white (cellulose-binding dye) demonstrated that RG-II exists throughout the primary cell wall. Finally, pulse labeling experiments

validate metabolic click-mediated labeling with Kdo-N₃ as an excellent tool to study the synthesis and redistribution of RG-II in cell wall.

The recent development of new click-compatible sugar analogues—glucose, galactose, fucose, arabinose, rhamnose, and sucrose [137,201]—allows a good opportunity to develop this technique and to improve our knowledge on polysaccharide biosynthesis and function as soon as the current limitations of the method can be bypassed. In fact, click chemistry relies on the reaction of azides and/or alkynes and uses copper as a catalyst; thus, it does not allow dynamic imaging of living cells as copper is toxic for cells. Hopefully, alternative methods, termed “copper-free click chemistry”, are currently being developed and have been successfully used to detect sugar analogues in living organisms using cyclooctyne (Figure 12B). For instance, the difluorinated cyclooctyne (DIFO) possesses ring strain and electron-withdrawing fluorine substituents that together promote dipolar cycloaddition with azides without the use of copper. The kinetics of the reaction are comparable to those of the copper-catalyzed reaction and it proceeds within minutes on living cells with no apparent toxicity. This method has been successfully used to label glycan in Chinese Hamster Ovary (CHO) cells [133] in mouse [202] and in plant [137] with no apparent toxicity, and allows us to consider new promising and attractive applications for direct imaging of glycan in living cells.

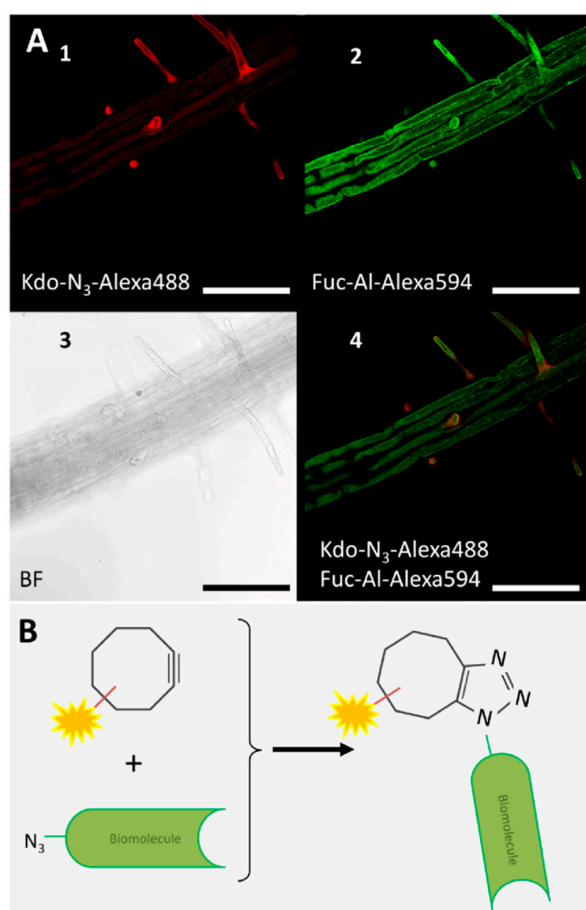


Figure 12. Click chemistry for in vivo plant labeling. (A) Double labeling of four day-old *Arabidopsis* seedlings incubated with 50 μ M of Kdo-Azide (Kdo-Az) and 50 μ M of Fucose-Alkyne (Fuc-AI) and successively labeled with Alexa Fluor[®] 488-alkyne (red) and Alexa Fluor[®] 594-Azide (green). (1) Elongation and differentiation zone observed with the A488 channel. (2) Same zone as in (1) observed with the A594 channel. (3) Bright-field image of the elongation zone. (4) Elongation zone observed with merged A488 and A594 channels. Scale bars: 100 μ m. (B) Schematic representation of the copper-free bioorthogonal reaction between an azido-biomolecule and a cyclooctyne-fluorophore.

4. Progress in Synthesis of Organic Fluorescent Probes

Nature produces few fluorescent secondary metabolites such as umbelliferone (coumarin skeleton), flavanols, curcumin, and hypericin which have been employed (natively or after modification) for bioimaging (Figure 13A) [203,204]. Since the discovery of natural Green Fluorescent Protein (GFP), many others have been discovered; however, they are now being engineered, allowing the production of differently colored proteins (see also Section 2.3).

To expand the library of fluorescent molecules, synthetic chemists have generated numerous new fluorescent scaffolds such as bimanes, bodipys, cyanines, squaraines, and xanthenes (fluorescein and rhodamines), to name the most well known (Figure 13B,C) [205–208]. These small molecules have had a huge impact on modern Life Sciences as they have allowed observation of living organisms, thanks to the development of bioimaging [208].

To further improve the photophysical characteristics of fluorescent molecules including brightness and photostability, concomitantly with new imaging approaches, new chemical strategies have been formed [209], taking into account that an ideal fluorophore (“the fluorescent grail”) should absorb and emit light with maximum efficiency, be photo- and chemically stable in biological medium, be of the smallest possible size, and be nontoxic [210].

As the size of the fluorophore matters if one wants to limit perturbations brought to the observed system, the very small bimane fluorophore has been developed and mostly used for accurate measurements of dynamics of proteins by FRET [211].

With a larger size, bodipy fluorophores presenting a rigid neutral system have been widely used thanks to their easy functionalization with maleimides or NHS esters, allowing introduction of targeting or hydrosolubilizing moieties. The bodipys are usually photostable and present a high quantum yield, but with a small Stokes shift. They can be found in commercially available dyes such as ER- or Lyso-trackers (Table 1) [212].

The cyanine family represents a very important class of fluorophores with multiple colors up to NIR, allowing multiplexing, FRET, or derivatization as chemosensors for analytes. They, however, generally suffer from photobleaching and small Stokes shift [213,214]. Cyanines can be found in commercially available dyes such as Mitotracker (Table 1).

Squaraine-type dyes are characterized by the presence of a four-membered ring bearing two ketones (squaric acid) out of which one or two may be enolized. The substitution of this cycle by electron-donating substituents, usually aromatic rings, makes the donor–acceptor–donor cyanin-type structure (see Figure 5). Due to their very rigid structure, they present an exceptionally high extinction coefficient, a large two-photon absorption cross section, and a very short Stokes shift; however, they usually suffer from instability in biological medium due to nucleophilic attack. To circumvent this issue, squaraine protected by a rotaxane ring has been developed, leading to very bright and stable dyes for cell imaging [215,216].

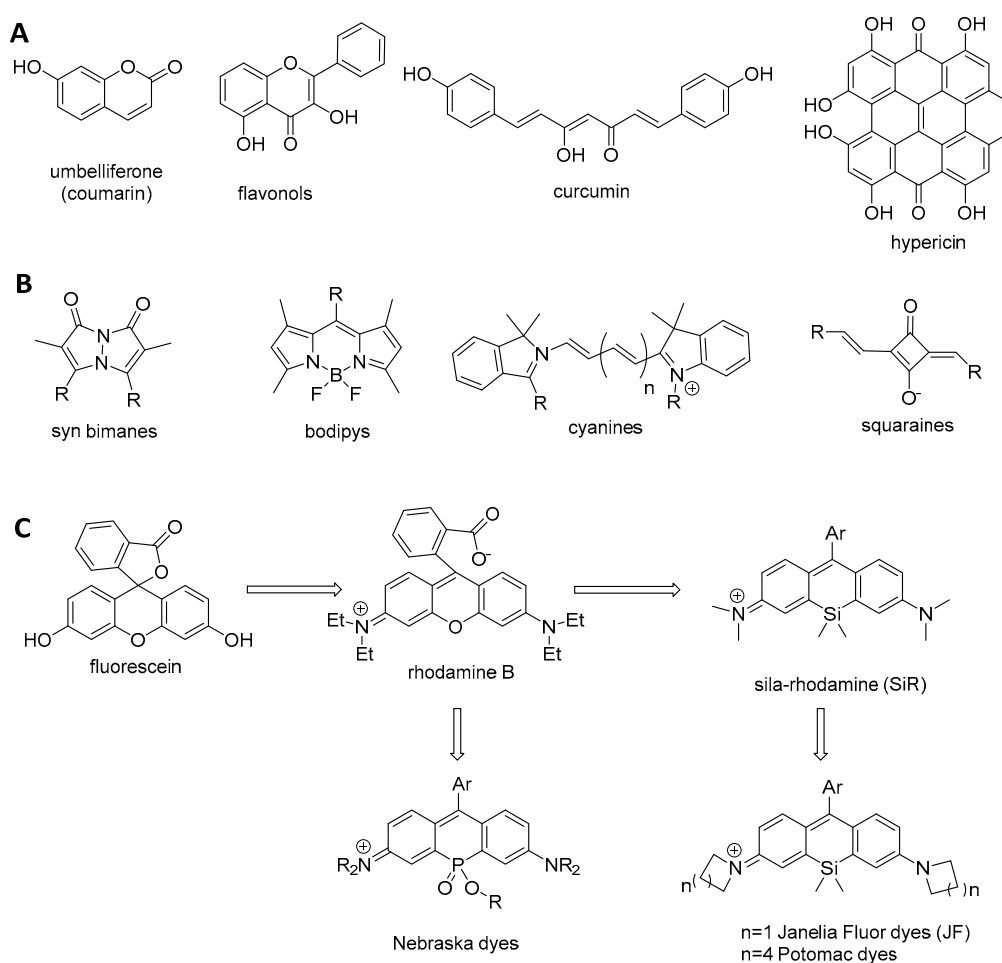


Figure 13. Examples of natural and synthetic fluorescent probes. (A) Fluorescent natural products; (B) Representative families of fluorophores; (C) Synthetic xanthene dyes derived from fluorescein.

4.1. Development of Small Near-Infrared Organic Molecules to Reduce Fine Cytotoxicity and to Image Thicker Samples

Among the synthetic modifications of known fluorophores, evolution of the skeleton of fluorescein is representative of the recent impact of chemistry on the conception of dyes. Indeed, fluorescein is a relatively simple tricyclic molecule possessing two phenols, with absorption and emission wavelengths of around 490 and 510 nm (Figure 13C). The replacement of phenols by amines or dialkylamines led to the development of the rhodamine dye family with absorption/emission wavelengths of 543/565 nm for rhodamine B (Figure 13C) [217]. Modifications of the skeleton with the introduction of silicon in rhodamines led to the development of Sila-Rhodamines (SiR) as powerful near-infrared (NIR) probes [218–220]. The replacement of O by Si in rhodamines leads to a red shift of both absorption and emission wavelengths resulting from a lowering of the excited state energy levels. Further modifications of substituents on the nitrogen atoms led to the development of Janelia Fluor [221] (azetidines) and Potomac dyes (azepanes) [220], which have superior brightness and stability to SiR. Similarly, replacement of O by phosphorus atom in rhodamines led to the development of Nebraska dyes [222] or others [223] also displaying NIR fluorescence (Figure 13C).

Some of the fluorescent dyes used for bioimaging have high affinity for a specific organelle due to their nature (polarity, charge, etc.) or to the presence of a targeting agent. Among the commercially available and widely used markers, specific stains can be found for cell nucleus (DAPI or Hoechst 33342), acidic organelles (LysoTrackers), endoplasmic reticulum (ERTrackers), or mitochondria (Mitotracker). They can also be chemically modified to act as a profluorophore that an enzymatic or

chemical reaction will convert back into the fluorophore (leading to an OFF \rightarrow ON signal), thus acting as chemosensors for analytes or as proof of biological activity (Table 1). Among these fluorophores, epicocconone, an azaphilone natural product isolated from the *Epicoccum nigrum* fungus, emerged as a profluorescent natural product that has been extensively used for protein staining on electrophoresis gels and for bioimaging [224] (Figure 14). Due to its water solubility, low molecular weight, nontoxicity, and cell permeability, epicocconone showed strong potential for live cell imaging [89,113]. The chemical synthesis, guided by DFT and photophysical studies, led to the development of a synthetic analogue with improved photostability and to epicocconone–hemicyanine hybrids with NIR emission [225–231].

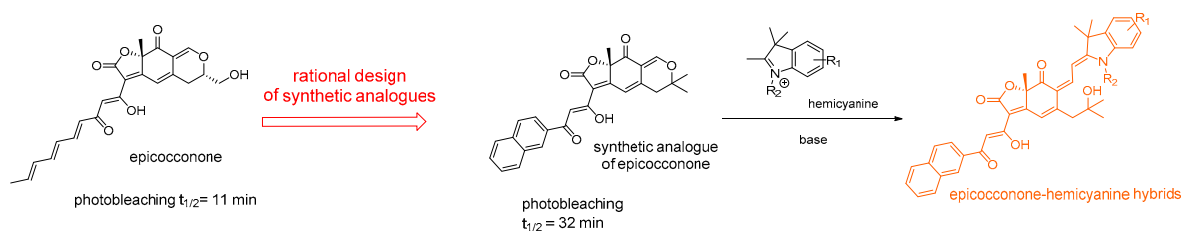


Figure 14. Epicocconone, synthetic analogues, and hybrids.

In bioimaging, epicocconone and its naphthyl analogue were compared through one-photon (1P) and two-photon (2P) advanced light microscopy studies using PC12 cells [113]. Results obtained with the synthetic analogue on PC12 cells showed more interesting characteristics than the natural product in terms of band sharpness, fluorescent intensity, photobleaching (fluorescence is only 25% weaker after a 30 min acquisition), and Stokes shift in 1P and 2P microscopies (Figure 15A).

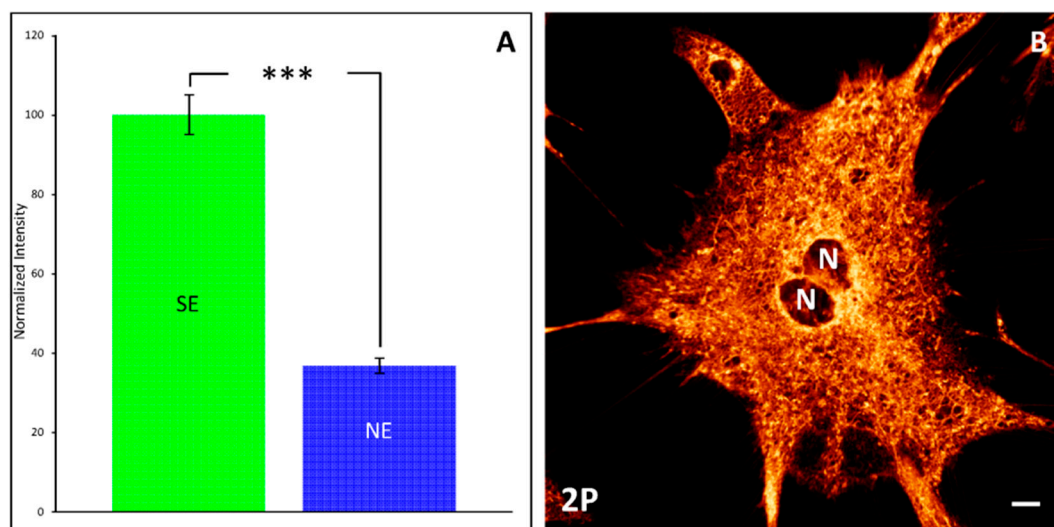


Figure 15. Characteristics of synthetic epicocconone (SE) and natural epicocconone (NE) through nonlinear optical microscopy. **(A)** Comparison of fluorescence intensity obtained by cell imaging with synthetic analogue of epicocconone (SE) and the natural product epicocconone (NE). *** $p < 0.001$ vs. SE. **(B)** Cell labeling with the naphthyl analogue of epicocconone through 2P microscopy. N = Nucleus. Scale: 10 μm . Modified with permission from [113]. Copyright 2017 Elsevier.

The synthetic analogue did not label the nucleus of the PC12 cell but induced a moderate labeling of plasma and nuclear membranes and of filamentous structures in the cytoplasm, and an intense labeling of numerous intracellular vesicle-like structures around the nucleus (Figure 15B). The skeleton of epicocconone could be further modified by making epicocconone–hemicyanine hybrids, based on an internal charge transfer (ICT) between different hemicyanine groups as electron donors and the naphthylketoenol group of the previous synthetic analogue as electron acceptor (Figure 14). Unlike epicocconone or its naphthyl analogue, this epicocconone–hemicyanine hybrid is natively fluorescent

with emission wavelengths red-shifted to the NIR region. It was shown that the hybrids have in general a large Stokes shift (about 80 nm) and an emission maximum ranging from 715 to 795 nm, depending on the nature of the hemicyanine moiety [225].

4.2. Development of Organic Probes to Increase Resolution in Microscopy

In wide-field and confocal microscopy, a single fluorophore can only be precisely localized if it is separated by a few hundred nanometers from others, due to the diffraction of light (see also Section 2.3). With regards to emission depletion and stochastic reconstruction principles, photophysical properties of probes have been recently reassessed to find the most valuable chromophores [232].

4.2.1. Development of Organic Probes for STED Nanoscopy

When used in a STED nanoscopy set up, fluorophores are exposed to the high intensity of the laser beam (see also Section 5) used to narrow the fluorescence into a very small volume; therefore, one of the key parameters of a STED fluorophore is photostability. A variety of mechanisms may lead to photodamage as excited-state absorption can produce chemically unstable upper energy states. Degradation is even more pronounced if triplet states are involved due to their long lifetime and their ability to generate highly reactive ROS and radicals [233]. These latter reactive species lead also to biological photodamage [234,235]. Other photobleaching effects are isomerization, oxidations, or reductions often leading to blue-emitting photoproducts, or the formation of twisted states. All these effects lower the fluorescence quantum yield. Another parameter is the Stokes shift, as the STED irradiation wavelength has to be different enough from the fluorophore excitation wavelength to avoid excitation of the fluorophore during the depletion step [96]. Therefore, when choosing a fluorophore, the equipment specification also has to be taken into consideration as the fluorescence wavelength should match the STED depletion wavelength [236]. The photophysical properties of many available fluorophores were assessed for STED nanoscopy [96]. In order to be effective and to avoid a strong fluorescent background, nanoscopy probes have to be specific. On the one hand, some fluorophores can be activated only by interaction with specific biomolecules; for example, a ruthenium complex was used to image DNA [237]. On the other hand, STED probes can be fluorophore-targeting agent conjugates, the most widespread targeting agents being antibodies even though they necessitate working with fixed cells. Live cell imaging requires a targeting agent able to internalize in cells, such as taxanes that allow the imaging of tubulin in living tissues [238], and biarsenical dyes [147], benzylguanines/benzylcytosine [144,239], and synthetic ligands [149] that were used for tetracysteine tag, SNAP/CLIP, and HaloTag fusion protein labeling, respectively. The stability of fluorophores, and, hence, their efficacy, also depends on their cellular environment as biological processes may damage excited chromophores. A good answer can be to localize fluorophores in hydrophobic cell compartments [240] or to encapsulate them in protecting fluorogen-activating peptides (FAPs) [241]. Hell's group from the Max Planck Institute for Biophysical Chemistry (Göttingen, Germany) is currently undertaking molecular engineering to provide optimized fluorophores. While these molecules have been, at this point, only assessed on fixed cells due the use of immunolabeling, they seem very promising for live cell imaging (Figure 13). Rhodamines were modified to improve their photostability and their ability to internalize in cells (Figure 16A).

Table 1. Classification of fluorescent probes for live cell imaging with regard to their applications in different type of living samples.

Application	Type of Sample	Method of Labelling	Probes (Non Exhaustive)	References (Non Exhaustive)
Cell viability	isolated cell or multi cell layers	permeation	Calcein-AM	[109,110,175]
	isolated cell or multi cell layers	permeation	acetate derivatives of fluorescein (FDA)	[110,111]
	organ	permeation	Syto 61, Sytox Orange, TO-PRO-1/3	[173,174]
Cell tracking	isolated cell/organ/organism	permeation/injection	CellTracker/Dil/Cyto-Tracers/WGA	[114,116,176,179,185,186]
	isolated cell	incorporation in lipid membrane	CellVue, CytoID Red	[115–117]
	isolated cell/organ/organism	infection (lentivectors)	Cyto-Tracers	[132]
	organ/organism	injection	Dextran-conjugated/SiR	[182,188]
	organism	transfection/electroporation	Plasmid construction	[140,141]
Identification of membrane, organelles and macromolecules				
plasma membrane	isolated cell/organ/organism	reversible binding	WGA	[114,122]
plasma membrane	organ	reversible binding	IB4	[174]
cytoskeleton	isolated cell/organ	permeation	SiR-Actin/Tubulin/Taxanes	[130,131,237]
nucleus	isolated cell or multi cell layers	permeation	Hoechst/SYTO/Nuc/dinuclear RuII-based complex 1 ⁴⁺	[112,113,123,124,237]
mitochondria	isolated cell/organ/organism	permeation	Mitotracker	[125–127,187]
lysosome	isolated cell/organ/organism	permeation	Lysotracker, SiR-Lysosome	[128–131]
glycan	isolated cell/organ/organism	click chemistry	azide or alkyl monosaccharide	[133,134,201]
plant primary cell wall	isolated cell/organ/organism	click chemistry	azide or alkyl monosaccharide	[135,137,197,200]
plant secondary cell wall	isolated cell/organ/organism	click chemistry	azide or alkyl monolignol	[198]
Cellular activity				
potential membrane activity	isolated cell	permeation	JC-1	[160]
ionic indicator	isolated cell or multi cell layers	permeation	fluo-4 (Ca ²⁺), SBFI (Na ²⁺), Fluo-Zin, KMG-20/27	[151–154,156–158]
ionic indicator	multilayers, organ	permeation	oregon green (Ca ²⁺)	[176,177]
ROS detection	isolated cell or multi cell layers	permeation	H2DCFDA, RedocSensor, SiR-NO, . . .	[160–163]
caspase activity	isolated cell or multi cell layers	permeation	FITC-ZVAD-FMK	[110]
plamid construction/Biosensors	isolated cell	transfection	GFP family or derivative protein	[140,165]
plamid construction/Biosensors	organ/organism	transfection by electroporation	GFP family or derivative protein	[181,189,190]
pathway signal transduction	isolated cell	infection (bacculovirus)	BacMam system	[113]
pathway signal transduction	isolated cell	transfection	FRET Biosensors	[166–171]
pathway signal transduction	organ	infection (HSV)	Biosensors	[179,180]

The best improvements were obtained through the introduction of side chains bearing phosphonates or hydroxyl groups and substitution of the lateral aromatic ring (Figure 13A). On the other hand, rigidification of the amino moieties improves fluorescence by preventing the formation of twisted low-emitting states [242]. Hell's group also modified coumarins and higher stability was obtained by introducing a new photostable electron-withdrawing group based on an original betaine structure [243] (Figure 16B). These coumarins are of particular interest as they feature high Stokes shift due to their “push–pull” nature, allowing two-color STED images when combined with rhodamines.

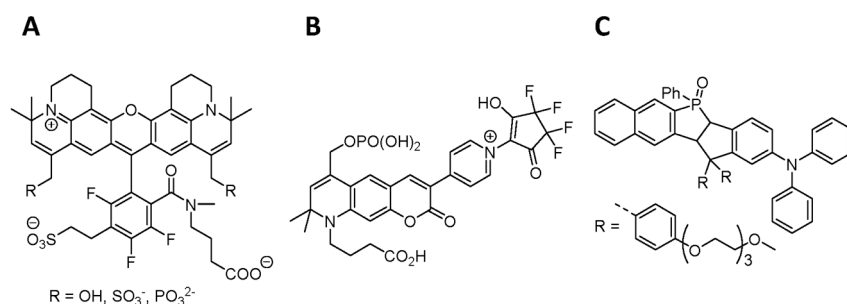


Figure 16. Optimized fluorophores for STED nanoscopy. (A) Rhodamine; (B) Coumarin; (C) Phosphole P-oxide.

Although only one STED wavelength is applied, the fluorophores are discriminated thanks to their very distinct excitation wavelengths. The quest for new optimized chromophores leads to exploring new chemical structures, e.g., a phosphole P-oxide-based chromophore showed promising photostability for application as a STED probe [244] (Figure 16C). The stability of fluorophores can be improved by encapsulation with dendrimers [245] or rotaxanes [215] which prevent reaction of excited-state chromophores with biological molecules. An alternative approach to more photostable structures consists of healing bleached chromophores thanks to antifading agents. These agents can be triplet states, or redox or radical quenchers used as additives during fluorescence imaging. However, their efficiency is related to their ability to interact quickly with bleached chromophores; this requires a high concentration which can disturb biological media. This could also be achieved by directly attaching the photostabilizing agent to the fluorophores to obtain self-healing chromophores [246]. Plasmonic nanoparticles can also be used to improve STED nanoscopy, as they have the ability to concentrate the light electromagnetic field in their vicinity. As a result, they allow a reduction in the power of irradiation depletion used to switch off the fluorescence of grafted fluorophores, including less photodamage to biological tissues [247].

4.2.2. Development of Organic Probes for Stochastic Approaches

As described previously (Section 2, Figure 8), stochastic techniques are classified into two main categories: those using photoactivable fluorophores, which are then destroyed under irradiation, and those relying on switchable fluorophores, which can be reversibly activated and deactivated. Among the first category, the PALM technique was introduced in 2006, and is based on the use of photoactivable fluorescent proteins (Pa-GFP, Pa-mcherry) or photoactivable “small molecule” fluorophores [248] (Figure 17A). In the second category, the STORM technique relies on reversible photoswitching; it was originally developed using Cy5 fluorophores reversibly switched off to a dark state thanks to a photo-triggered reaction with biological thiols [100,249,250]. This approach can be generalized to the majority of cyanine fluorophores commonly used in classical fluorescence imaging. Other common fluorophores derived from rhodamine were also used, the dark state being generated from diverse mechanisms like photoredox reaction or the formation of long-living triplet states [251]. However, these small molecules systems are limited due to their “switching fatigue”; to date, photoswitchable fluorescent proteins are the most stable photoswitching systems [252]. In

an effort to close this gap, new fluorophores based on diarylethene structures selected for their photochromic behavior were synthesized by Hell's group [253] (Figure 17B).

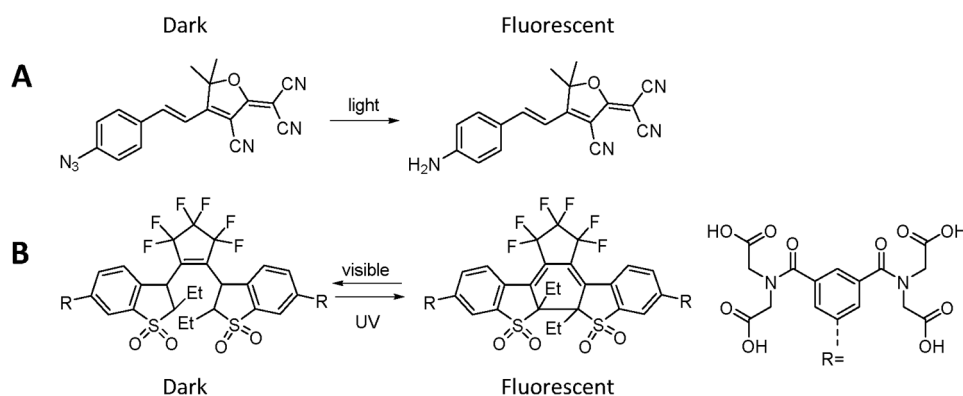


Figure 17. Fluorophores for stochastic fluorescent imaging. (A) Photoactivable fluorophore by photoreduction; (B) Photoswitchable diarylethene fluorophore.

Small organic fluorophores are complementary to bioengineered fluorescent proteins. Small molecules may lack solubility, or suffer from uncontrolled biodistribution or enzymatic instability. One of the main challenges with small molecules is targeting. Indeed, monoclonal antibodies are the most commonly used targeting agent for small molecules in fixed cells due to their high specificity; however, they are not able to internalize in living cells. Therefore, other targeting agents have been developed to cope with this problem, such as lectins [122], or drugs like Paclitaxel [238]. On one hand, FPs directly expressed inside cells do not present this problem, but require bioengineering preliminary work to obtain appropriate proteins; the introduction of such large tags may modify the activity or the structure of imaged proteins. On the other hand, small molecules are easier to modify, and can be built as a platform combining both imaging and biological properties or other functionalities, i.e., “Fluorescent False Neurotransmitters” [254], photoclick labeling dyes [255], and profluorescent ligands of genetically encoded tags [256,257].

5. Generation, Collection, Detection, and Analysis of the Fluorescence Signal from Living Samples

As proposed by the PSI triad concept with interrelationship between pillars, general improvement of the fluorescence signal is the result of better probes detected with adapted and efficient instruments. Consequently, specialist knowledge of light sources, objectives, detectors, and image processing is also essential to optimize live cell imaging.

5.1. Light Sources

Originating from a light source that can be a mercury/xenon arc lamp, a light-emitting diode (LED), or a continuous or pulsed laser, photons are absorbed by the probe that emits in return a signal of fluorescence. Considering the adverse effects of phototoxicity [258] and photobleaching on cell activity and time-lapse duration, a comparison of light source characteristics is presented here (Table 2). A first group of sources with low light power is represented by supercontinuum sources. Supercontinuum lasers, also called “white lasers”, which result from the dispersion of a continuous laser (1032 nm) into a nonlinear material (crystal fiber), offer a broad spectral band of light emission (250–1100 nm) with low laser power (<5 mW) [259]. A second group of light sources with moderate to high (5–500 mW) light power is represented by gas lasers, arc lamps, diode lasers, and LEDs [260]. The third group comprises depletion lasers for STED nanoscopy and solid-state lasers like Ti-sapphire lasers dedicated to two-photon absorption applications. Tunable pulsed Ti-sapphire lasers emit light in the range of 680 to 1080 nm with high power (up to 4 W) [261]. Consequently, electro- or acousto-optic modulators (EOM and AOM) are necessary to reduce the light power which is delivered to living

samples. Therefore, phototoxicity and photobleaching are significantly reduced with supercontinuum lasers. High-power solid-state lasers may induce large phototoxicity and photobleaching but in a restricted focal volume due to the two-photon principle. In contrast, they have the advantages of emitting red and near-infrared photons that are less cytotoxic. Probe and living sample preservations could also be optimized by reducing the pixel time, i.e., limiting the duration of laser impact on a pixel through an increase in rotation speed for spinning disk microscopy [262] or scanning speed (resonant scanner) in confocal/2P microscopy [36]. Exposure of living samples to light is also a major issue in nanoscopy approaches. For STED nanoscopy, the power of the depletion laser might be deleterious for cellular structures [122]. However, depletion with new wavelengths in near-infrared or with pulsed infrared lasers is preferred for live cell imaging [263]. The applications of stochastic nanoscopies to living samples are for the moment limited by the duration of the acquisition [264]. Structured illumination microscopy (SIM), which is compatible with most standard fluorophores, offers interesting resolutions between 50 and 100 nm but can also be limited in time resolution due to numerous pattern acquisitions [264].

Table 2. Comparison of characteristics of light sources currently used for live cell imaging. Special focus has been given to phototoxicity and photobleaching induced by light sources.

Light Source	Wide-Field Microscopy			Advanced Light Imaging Approaches				
	Mercury Arc Lamp	Xenon Arc Lamp	LED	Laser 1P		Laser 2P	STED	
	Liquid light guide/Direct coupling			Gas	Diode	Supercontinuum	Solid-State	Depletion
Power range (mW)	100–300	3000–5000	50–500	5–20	10–50	0.5–5	700–4000	1500–2000
Maximum power (mW)	2 *	25 *	250 *	5 *	8 *	0.45 *	2850 **	300–450 ***
Living Cells	Phototoxicity	++	+++	++++	++	+	+++++	+++++
	Photobleaching	+++	++++	+++++	+++	++	+	+++++

+, very low; ++, low; +++, moderate; +++++, high; ++++++, very high. Laser 1P = one-photon continuous laser. Laser 2P = two-photon pulsed laser. Power measurements were obtained with a power meter (Thorlabs PM100D + S170C Sensor) in the absence of objective. * power measurement at 488 nm; ** power measurement at 800 nm; *** power measurement at 592 nm.

5.2. Objectives

For observation of living samples (isolated cells, tissue slices, organs, or organisms) and fluorescence signal collection, the choice or the strain of the objective is a major issue. Dry, multi-immersion, oil, water, and glycerol objectives are available (Figure 18) [263]. The first rule is to respect as much as possible the refractive index between the aqueous incubation medium of the sample and the immersion medium of the objective. Consequently, water ($n = 1.33$) and glycerol ($n = 1.3$) objectives are more adapted for live cell imaging [265]. Due to repetitive movements or medium evaporating during long-time/multiposition acquisitions, dry objectives are nevertheless preferred despite their poor optical characteristics. More recently, commercial recurring refilled water systems have been developed to optimize water-objective images during long time lapses at 37 °C. The second rule is to consider the numerical aperture (NA) of the objective with regard to the requirements of signal collection, resolution, working distance (WD), and depth of field (DF). For high photon collection and high resolution, objectives with large NA ($1.2 < NA < 1.49$) are preferred in particular for intracellular localization purposes (Figure 18) [266]. Some objectives are also equipped with a correction collar to limit image aberration due to fluctuations in cover glass thickness, temperature, and specimen inhomogeneities [267]. In contrast, small NA ($0.02 < NA < 0.8$) objectives with large WD and DF are used for tissue slice or organism studies (Figure 18) [111,268]. It is also interesting to verify that the emission spectrum of the fluorescent probe completely fits with the transmission curve of the objective. Finally, autofocus systems might be helpful for mid-length and long time lapses [269]. For nanoscopy, new objectives with WD and DF up to 300 and 150 μm now facilitate STED approaches in living tissues [269]. Therefore, depending on the type of sample and the scientific question, the choice of the objective is crucial to appropriately detecting the fluorescence signal of interest.

Objective	Magnification: x2-x5 Dry NA: from 0.02 to 0.5 WD: from 1.9 to 9.7 cm	Videomacroscopy Confocal macroscopy	Instrument
	Magnification: x10-x20-x40 Dry NA: from 0.2 to 0.8 WD: from 0.3 to 8 mm	Videomicroscopy Plate-reader/Imager Light sheet microscopy	
	Magnification x10-x20-x40 Water Immersion NA: from 0.3 to 1 WD: from 2 to 4 mm	Confocal microscopy Multiphoton microscopy	
	Magnification: x10-x20-x40 Oil immersion NA: from 0.2 to 0.8 WD: from 100 to 500 μm	Videomicroscopy Confocal microscopy Spinning disk confocal microscopy	
	Magnification: x60/63-x100 Water/Glycerol Immersion NA: from 1.2 to 1.3 WD: from 100 to 300 μm	Confocal microscopy Nanoscopies	
	Magnification: x60/63-x100 Oil Immersion NA: from 1.4 to 1.49 WD: from 90 to 150 μm	Videomicroscopy Confocal microscopy Spinning disk confocal microscopy Multiphoton microscopy Nanoscopies	

Figure 18. Characteristics of objectives used for live cell imaging. Special focus has been given to immersion medium, numerical aperture (NA), and working distance (WD).

5.3. Detectors

Depending of the type of imaging system (wide-field, spinning disk, confocal, 2P, nanoscopy, etc.), single-point or array detectors are used for fluorescence signal detection [7]. Different key parameters have to be considered for each type of sensor. Single-point detectors such as photomultiplier tubes (PMTs) and hybrid photodetectors (HPDs) have to be compared with regard to their quantum efficiency (QE), their signal-to-noise ratio (SNR) value, and their time response [7]. Since HPDs combine the advantages of the vacuum technology of PMT and avalanche photodiode semiconductor diode (APD) technology, they offer low-light detection ($\times 1.3$ – 1.4), especially for single molecule detection, excellent timing resolution ($\times 2$ – 3), and noise close to 0 [269]. Due to semiconductor diode technology, a photon counting mode is also available with HPD, allowing direct fluorescence quantification [270]. In contrast to single-point detectors, there is a large diversity of array detectors that can be distributed into three groups: Charge-Coupled Device cameras (CCD), Electron-Multiplication CCD cameras (EM-CCD), and scientific Complementary Metal Oxide Semiconductor (sCMOS) cameras [270]. For live cell imaging, criteria such as frame rate, QE, SNR, and pixel size are generally compared to reach appropriate temporal and spatial resolution. CCD cameras appeared almost 50 years ago with continuous development since then for time response and QE. Consequently, EM-CCD cameras were developed for the detection of low fluorescence signals, in particular for *in vivo* applications with back-illuminated sensors [271]. Nowadays, sCMOS cameras allow larger field of view than other sensors, small pixel size, and a very good SNR [272]. With a rapid frame rate, they are fast sensors compared with CCD and EM-CCD cameras and have equivalent or lower QE [270]. Taken together, scientific requirements such as spatial and temporal resolution and low fluorescence signal may be decisive for the choice of array detector.

5.4. Instrument Performance

As described in the above paragraphs, light sources, objectives, scanners, and detectors are key elements for appropriate live cell imaging with fluorescent probes. Consequently, the stability and performance of these elements during acquisition are essential to obtaining experimental reproducibility and repeatability of confident measurements [273]. Thus, regular control of laser power, field illumination, and detector sensitivity over time is a requirement of performing successful experiments. In the context of acquisition of one shot or short time lapses, field illumination and detector sensitivity should be stable (Table 3).

Table 3. Potential instrumental instabilities during one-time acquisition, and short and long time lapses.

Instrumental parameter	Duration of Acquisition		
	One-Time Acquisition (s or few min)	Short Time-Lapse (tens of min)	Long Time-Lapse (several hours)
Power Laser	-	+	+++
Field of Illumination	-	-	-
Detector Sensitivity	-	-	-
Drift and Shift (x,y,z)	-	++	++++
Temperature and CO ₂	+	++	++++

-, no risk; +, low risk; ++, moderate risk; +++, high risk; +++++, very high risk.

In contrast, instability of laser power may appear in mid-length or long time lapses [273]. Similarly, environmental and room temperature as well as *xyz* positioning may vary during mid-length and long time-lapses. Please note that variations of temperature are often responsible for variations of stage drifts [273,274]. Such variations can be controlled by introducing focus-keeping systems for long-term monitoring, limiting loss of information [267]. When required, saturation of the local atmosphere with CO₂ (5%) can be achieved by an automatic gas mixer or home-made systems. Variations of environmental temperature and CO₂ concentration induce biological artifacts that can lead to misinterpretation of the results.

5.5. Image Processing

Imaging living samples together for as long as possible while preserving the fluorescence signal from photobleaching is a major issue. In this context, compromises of intensity of light sources, time of exposure or time of scanning, and signal amplification methods are mandatory. These compromises generally lead to degradation of the image quality with an increase of the noise and, consequently, a decrease in SNR. The degradation can be assumed, giving priority to biological sample integrity and long life of the fluorescent probe. However, to overcome the noise, image processing through deconvolution has several advantages leading to an increase in SNR, contrast, and resolution (Figure 19). Thus, deconvolution is of main importance in nanoscopy but also in confocal and wide-field microscopy with algorithms that integrate the characteristics of the optical system (objective, NA, immersion medium, etc.). Nevertheless, successful deconvolution requires rigorous backward imaging acquisition with appropriate sampling in x , y , and z dimensions according to the Nyquist criterion. In addition, pitfalls of acquisition such as mechanical drift and shift, spectral crosstalk of fluorescent probes, and saturation of the signal must be strictly eliminated.

Degradation of image quality should, however, be limited for tracking experiments, in particular in organotypic slices, organs, and organisms due to the risk of lost cells, organelles, or molecules during time lapse. Consequently, detection of “objects” over time should be improved through commercial or open source image processing programs [275]. In particular, deconvolution and combination of morphologic filters (erosion, dilatation, etc.) facilitate the efficiency of automatic or semi-automatic tracking [268]. However, home-made strategies with dedicated algorithms are often necessary to fully match with the expected results [276,277].

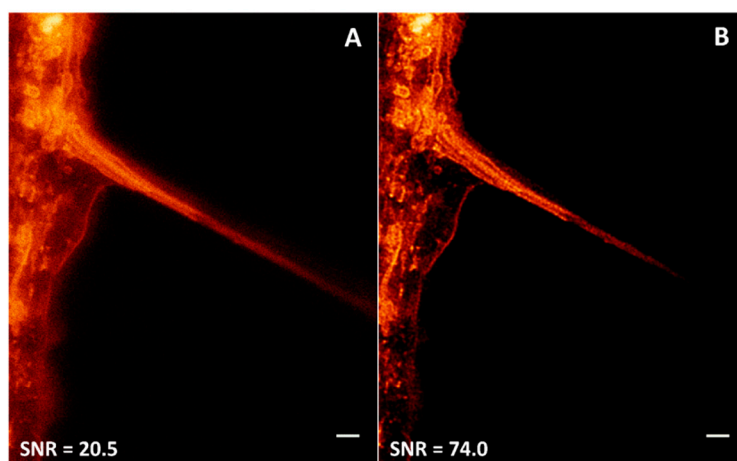


Figure 19. Improvement of Signal-to-Noise Ratio (SNR) in STED images through deconvolution. Alexa 488-WGA-labeled Tunneling NanoTubes in living PC12 cells were observed through CW gated STED (for experimental procedures, please see [122]). (A) Raw image; (B) Deconvolved image through Huygens professional® 18.04. Values of SNR were determined through ImageJ software (Rasband, W.S., U.S. National Institutes of Health, Bethesda, MD, USA, 1997–2016). Scale bar: 1 μm .

6. Conclusions

One of the roles of CIPs is to support researchers from both the public and private sectors in their choice of adapted fluorescent probe for their scientific projects. In addition, CIPs closely work with research laboratories that develop new strategies to improve the fluorescence properties of probes including targeting and adaptation to advanced imaging technologies (2P microscopy, STED nanoscopy, etc.).

The progress made in chemistry, optics, electronics, and fluorescence microscopy techniques has allowed the frontiers of bioimaging of living samples to be pushed back. Chemistry has been and is still needed to provide molecules with higher stability and with photophysical properties compatible

with the use of high-energy lasers. While conventional 1P and 2P microscopies are routinely used in bioimaging, many techniques are now being developed for nanoscopy that will allow a deeper understanding of biological processes. The progress of DFT calculations and the development of new synthetic methodologies allow the synthesis of rationally designed small fluorescent organic molecules, in particular, modification of a basic skeleton or introduction of new substituents aiming at gaining brightness, photostability, and selectivity in bioimaging along with tuning absorption and emission wavelengths.

For fluorescent labeling, both the bioavailability of the probe and the type of living sample have to be considered. Consequently, the method of labeling may be determined by the “cellular environment”, i.e., isolated cells, cells within an organotypic slice or organ, or cells within an organism. For that, a large diversity of labeling strategies from simple diffusion of cell-permeant probes to engineered fluorescent proteins expressed by animals, plants, or micro-organisms is available. Click chemistry that results from the ligation of non-natural metabolite derivatives with a fluorescent reporter is now widely used to visualize specific molecules, such as glycan and lipids, for which genetically encoded reporters are not possible.

Beyond classical spectral specifications of light sources and detectors to excite and to detect, respectively, a fluorescent probe, it is important to pay particular attention to instruments in the context of living samples. As a matter of fact, the tricky issue is to use low light power to preserve the sample as much as possible and to limit the photobleaching as much as possible while reaching appropriate spatial and/or temporal resolution. Consequently, the brightness and photostability of the fluorescent probes are preponderant parameters. In addition, we have shown in this review that the choices and performance of the instruments including the light sources (supercontinuum, diode, gas, and solid-state lasers) and the detectors (PMT, HyD, sCMOS, CCD, or EM-CCD), together with the mode of acquisition (resonant scanner, spinning disk), are crucial for live cell imaging. Light power can also be further reduced by developing specific post-acquisition image processing procedures such as deconvolution to achieve similar SNR and spatial resolution but with lower light exposure. Taken together, the concept of the Probe–Sample–Instrument (PSI) triad aims to identify the criteria that will help in making the appropriate choice of fluorescent organic probe for living cell studies.

Author Contributions: L.G. was the general manager of the review. T.G., S.L., L.G. and X.F. wrote Section 2. L.G., A.L. (Arnaud Lehner), M.B. and P.L. wrote Section 3. T.G., S.L. and X.F. wrote Section 4. L.G., D.S., M.B. and A.L. (Alexis Lebon) wrote Section 5. H.K. provided scientific support and helped revising the text.

Funding: This work was supported by Inserm, IRIB, Normandie Univ, IBiSA, the Normandy Region, UNIROUEN, the European Regional Development Fund (ERDF—PACT-CBS).

Conflicts of Interest: The authors declare no conflict of interest.

References

1. Tsien, R.Y. Constructing and exploiting the fluorescent protein paintbox (Nobel Lecture). *Angew. Chem. Int. Ed.* **2009**, *48*, 5612–5626. [[CrossRef](#)] [[PubMed](#)]
2. Chudakov, D.M.; Matz, M.V.; Lukyanov, S.; Lukyanov, K.A. Fluorescent proteins and their applications in imaging living cells and tissues. *Physiol. Rev.* **2010**, *90*, 1103–1163. [[CrossRef](#)] [[PubMed](#)]
3. Betzig, E. Nobel lecture: Single molecules, cells, and super-resolution optics. *Rev. Mod. Phys.* **2015**, *87*, 1153. [[CrossRef](#)]
4. Hell, S.W. Nobel lecture: Nanoscopy with freely propagating light. *Rev. Mod. Phys.* **2015**, *87*, 1169. [[CrossRef](#)]
5. Moerner, W.E. Nobel lecture: Single-molecule spectroscopy, imaging, and photocontrol: Foundations for super-resolution microscopy. *Rev. Mod. Phys.* **2015**, *87*, 1183. [[CrossRef](#)]
6. Sahl, S.J.; Hell, S.W.; Jakobs, S. Fluorescence nanoscopy in cell biology. *Nat. Rev. Mol. Cell. Biol.* **2017**, *18*, 685–701. [[CrossRef](#)] [[PubMed](#)]
7. Borlinghaus, R.T.; Birk, H.; Schreiber, F. Detectors for sensitive detection: HyD. In *Current Microscopy Contributions to Advances in Science and Technology*, 1st ed.; Mendez-Vilas, A., Ed.; Formatex Research Center: Badajoz, Spain, 2012; Volume 2, pp. 818–825.

8. Michalet, X.; Cheng, A.; Antelman, J.; Suyama, M.; Arisaka, K.; Weiss, S. Hybrid photodetector for single-molecule spectroscopy and microscopy. *Proc. SPIE Int. Soc. Opt. Eng.* **2008**, *6862*. [[CrossRef](#)]
9. Juris, A.; Balzani, V.; Barigelli, F.; Campagna, S.; Belser, P.; von Zelewsky, A. Ru(II) polypyridine complexes: Photophysics, photochemistry, electrochemistry, and chemiluminescence. *Coord. Chem. Rev.* **1988**, *84*, 85–277. [[CrossRef](#)]
10. Fernández-Moreira, V.; Thorp-Greenwood, F.L.; Coogan, M.P. Application of d6 transition metal complexes in fluorescence cell imaging. *Chem. Commun.* **2010**, *46*, 186–202. [[CrossRef](#)] [[PubMed](#)]
11. Zhao, Q.; Huang, C.; Li, F. Phosphorescent heavy-metal complexes for bioimaging. *Chem. Soc. Rev.* **2011**, *40*, 2508–2524. [[CrossRef](#)] [[PubMed](#)]
12. Andraud, C.; Maury, O. Lanthanide complexes for nonlinear optics: From fundamental aspects to applications. *Eur. J. Inorg. Chem.* **2009**, *2009*, 4357–4371. [[CrossRef](#)]
13. Sy, M.; Nonat, A.; Hildebrandt, N.; Charbonnière, L.J. Lanthanide-based luminescence biolabelling. *Chem. Commun.* **2016**, *52*, 5080–5095. [[CrossRef](#)] [[PubMed](#)]
14. Bünzli, J.C.G. Lanthanide luminescence for biomedical analyses and imaging. *Chem. Rev.* **2010**, *110*, 2729–2755. [[CrossRef](#)] [[PubMed](#)]
15. Chatterjee, D.K.; Rufaihah, A.J.; Zhang, Y. Upconversion fluorescence imaging of cells and small animals using lanthanide doped nanocrystals. *Biomaterials* **2008**, *29*, 937–943. [[CrossRef](#)] [[PubMed](#)]
16. Shen, J.; Zhao, L.; Han, G. Lanthanide-doped upconverting luminescent nanoparticle platforms for optical imaging-guided drug delivery and therapy. *Adv. Drug Deliv. Rev.* **2013**, *65*, 744–755. [[CrossRef](#)] [[PubMed](#)]
17. Dong, H.; Du, S.R.; Zheng, X.-Y.; Lyu, G.M.; Sun, L.D.; Li, L.D.; Zhang, P.Z.; Zhang, C.; Yan, C.H. Lanthanide nanoparticles: From design toward bioimaging and therapy. *Chem. Rev.* **2015**, *115*, 10725–10815. [[CrossRef](#)] [[PubMed](#)]
18. Reisch, A.; Klymchenko, A.S. Fluorescent polymer nanoparticles based on dyes: Seeking brighter tools for bioimaging. *Small* **2016**, *12*, 1968–1992. [[CrossRef](#)] [[PubMed](#)]
19. Mettra, B.; Appaix, F.; Olesiak-Banska, J.; Le Bahers, T.; Leung, A.; Matczyszyn, K.; Samoc, M.; van der Sanden, B.; Monnereau, C.; Andraud, C. A fluorescent polymer probe with high selectivity toward vascular endothelial cells for and beyond noninvasive two-photon intravital imaging of brain vasculature. *ACS Appl. Mater. Interfaces* **2016**, *8*, 17047–17059. [[CrossRef](#)] [[PubMed](#)]
20. Petryayeva, E.; Algar, W.R.; Medintz, I.L. Quantum dots in bioanalysis: A review of applications across various platforms for fluorescence spectroscopy and imaging. *Appl. Spectrosc.* **2013**, *67*, 215–252. [[CrossRef](#)] [[PubMed](#)]
21. Zhou, J.; Yang, Y.; Zhang, C. Toward biocompatible semiconductor Quantum Dots: From biosynthesis and bioconjugation to biomedical Application. *Chem. Rev.* **2015**, *115*, 11669–11717. [[CrossRef](#)] [[PubMed](#)]
22. Bilan, R.; Fleury, F.; Nabiev, I.; Sukhanova, A. Quantum Dot surface chemistry and functionalization for cell targeting and imaging. *Bioconjug. Chem.* **2015**, *26*, 609–624. [[CrossRef](#)] [[PubMed](#)]
23. Hong, G.; Diao, S.; Antaris, A.L.; Dai, H. Carbon nanomaterials for biological imaging and nanomedicinal therapy. *Chem. Rev.* **2015**, *115*, 10816–10906. [[CrossRef](#)] [[PubMed](#)]
24. Wolfbeis, O.S. An overview of nanoparticles commonly used in fluorescent bioimaging. *Chem. Soc. Rev.* **2015**, *44*, 4743–4768. [[CrossRef](#)] [[PubMed](#)]
25. Yao, J.; Yang, M.; Duan, Y. Chemistry, biology, and medicine of fluorescent nanomaterials and related systems: New insights into biosensing, bioimaging, genomics, diagnostics, and therapy. *Chem. Rev.* **2014**, *114*, 6130–6178. [[CrossRef](#)] [[PubMed](#)]
26. Lemke, E.A.; Schultz, C. Principles for designing fluorescent sensors and reporters. *Nat. Chem. Biol.* **2011**, *7*, 480–483. [[CrossRef](#)] [[PubMed](#)]
27. Suzuki, Y.; Yokoyama, K. Development of functional fluorescent molecular probes for the detection of biological substances. *Biosensors* **2015**, *5*, 337–363. [[CrossRef](#)] [[PubMed](#)]
28. Lewis, M.W.; Robalino, I.V.; Keyhani, N.O. Uptake of the fluorescent probe FM4-64 by hyphae and haemolymph-derived in vivo hyphal bodies of the entomopathogenic fungus *Beauveria bassiana*. *Microbiology* **2009**, *155*, 3110–3120. [[CrossRef](#)] [[PubMed](#)]
29. Levine, M.N.; Hoang, T.T.; Raines, R.T. Fluorogenic probe for constitutive cellular endocytosis. *Chem. Biol.* **2013**, *20*, 614–618. [[CrossRef](#)] [[PubMed](#)]

30. Chow, Y.T.; Chen, S.; Wang, R.; Liu, C.; Kong, C.W.; Li, R.A.; Cheng, S.H.; Sun, D. Single cell transfection through precise microinjection with quantitatively controlled injection volumes. *Sci. Rep.* **2016**, *6*, 24127. [[CrossRef](#)] [[PubMed](#)]
31. Sahoo, H. Fluorescent labeling techniques in biomolecules: A flashback. *RSC Adv.* **2012**, *2*, 7017–7029. [[CrossRef](#)]
32. Dean, K.M.; Palmer, A.E. Advances in fluorescence labeling strategies for dynamic cellular imaging. *Nat. Chem. Biol.* **2014**, *7*, 512–523. [[CrossRef](#)] [[PubMed](#)]
33. Fornwald, J.A.; Lu, Q.; Boyce, F.M.; Ames, R.S. Gene expression in mammalian cells using BacMam, a modified baculovirus system. *Methods Mol. Biol.* **2016**, *1350*, 95–116. [[PubMed](#)]
34. Icha, J.; Weber, M.; Waters, J.C.; Norden, C. Phototoxicity in live fluorescence microscopy, and how to avoid it. *Bioessays* **2017**, *39*, 1700003. [[CrossRef](#)] [[PubMed](#)]
35. Santi, P.A. Light sheet fluorescence microscopy: A review. *J. Histochem. Cytochem.* **2011**, *59*, 129–138. [[CrossRef](#)] [[PubMed](#)]
36. Chatterjee, K.; Pratiwi, F.W.; Wu, F.C.M.; Chen, P.; Chen, B.C. Recent progress in light sheet microscopy for biological applications. *Appl. Spectrosc.* **2018**, *72*, 1137–1169. [[CrossRef](#)] [[PubMed](#)]
37. Miller, D.R.; Jarrett, J.W.; Hassan, A.M.; Dunn, A.K. Deep tissue imaging with multiphoton fluorescence microscopy. *Curr. Opin. Biomed. Eng.* **2017**, *4*, 32–39. [[CrossRef](#)] [[PubMed](#)]
38. Van den Wildenberg, S.M.J.L.; Prevo, B.; Peterman, E.J.G. A brief Introduction to single-molecule fluorescence methods. *Methods Mol. Biol.* **2018**, *1665*, 93–113. [[PubMed](#)]
39. Combs, C.A.; Shroff, H. Fluorescence microscopy: A concise guide to current imaging methods. *Curr. Protoc. Neurosci.* **2017**, *79*. [[CrossRef](#)]
40. Turro, N.J.; Ramamurthy, V.; Scaiano, J.C. *Modern Molecular Photochemistry of Organic Molecules*; University Science books: Sausalito, CA, USA, 2010; p. 1120, ISBN 978-1-891389-25-2.
41. Lakowicz, J.R. *Principles of Fluorescence Spectroscopy*, 3rd ed.; Springer Science: New York, NY, USA, 2006; p. 954, ISBN 978-0-387-31278-1.
42. Valeur, B.; Berberan-Santos, M.N. *Molecular Fluorescence: Principles and Applications*; Wiley-VCH Verlag GmbH & Co. KGaA: Weinheim, Germany, 2012; p. 592, ISBN 978-3-527-65000-2.
43. Kivala, M.; Diederich, F. Acetylene-derived strong organic acceptors for planar and nonplanar push–pull chromophores. *Acc. Chem. Res.* **2009**, *42*, 235–248. [[CrossRef](#)] [[PubMed](#)]
44. Mishra, A.; Behera, R.K.; Behera, P.K.; Mishra, B.K.; Behera, G.B. Cyanines during the 1990s: A review. *Chem. Rev.* **2000**, *100*, 1973–2012. [[CrossRef](#)] [[PubMed](#)]
45. Taniguchi, M.; Lindsey, J.S. Database of absorption and fluorescence spectra of >300 common compounds for use in photochemCAD. *Photochem. Photobiol.* **2017**, *94*, 290–327. [[CrossRef](#)] [[PubMed](#)]
46. Yang, Z.; Cao, J.; He, Y.; Yang, J.H.; Kim, T.; Peng, X.; Kim, J.S. Macro-/micro-environment-sensitive chemosensing and biological imaging. *Chem. Soc. Rev.* **2014**, *43*, 4563–4601. [[CrossRef](#)] [[PubMed](#)]
47. Kim, Y.E.; Chen, J.; Chan, J.R.; Langen, R. Engineering a polarity-sensitive biosensor for time-lapse imaging of apoptotic processes and degeneration. *Nat. Methods* **2010**, *7*, 67–73. [[CrossRef](#)] [[PubMed](#)]
48. Signore, G.; Nifosi, R.; Albertazzi, L.; Storti, B.; Bizzarri, R. Polarity-sensitive coumarins tailored to live cell imaging. *J. Am. Chem. Soc.* **2010**, *132*, 1276–1288. [[CrossRef](#)] [[PubMed](#)]
49. López-Duarte, I.; Vu, T.T.; Izquierdo, M.A.; Bull, J.A.; Kuimova, M.K. A molecular rotor for measuring viscosity in plasma membranes of live cells. *Chem. Commun.* **2014**, *50*, 5282–5284. [[CrossRef](#)] [[PubMed](#)]
50. Haidekker, M.A.; Ling, T.; Anglo, M.; Stevens, H.Y.; Frangos, J.A.; Theodorakis, E.A. New fluorescent probes for the measurement of cell membrane viscosity. *Chem. Biol.* **2001**, *8*, 123–131. [[CrossRef](#)]
51. Vyšniauskas, A.; Balaz, M.; Anderson, H.L.; Kuimova, M.K. Dual mode quantitative imaging of microscopic viscosity using a conjugated porphyrin dimer. *Phys. Chem. Chem. Phys.* **2015**, *17*, 7548–7554. [[CrossRef](#)] [[PubMed](#)]
52. Ipuy, M.; Billon, C.; Micouin, G.; Samarut, J.; Andraud, C.; Bretonnière, Y. Fluorescent push–pull pH-responsive probes for ratiometric detection of intracellular pH. *Org. Biomol. Chem.* **2014**, *12*, 3641–3648. [[CrossRef](#)] [[PubMed](#)]
53. Gutscher, M.; Pauleau, A.L.; Marty, L.; Brach, T.; Wabnitz, G.H.; Samstag, Y.; Meyer, A.J.; Dick, T.P. Real-time imaging of the intracellular glutathione redox potential. *Nat. Methods* **2008**, *5*, 553–559. [[CrossRef](#)] [[PubMed](#)]
54. Gross, D.; Loew, L.M.; Webb, W.W. Optical imaging of cell membrane potential changes induced by applied electric fields. *Biophys. J.* **1986**, *50*, 339–348. [[CrossRef](#)]

55. Barsu, C.; Cheaib, R.; Chambert, S.; Queneau, Y.; Maury, O.; Cottet, D.; Wege, H.; Douady, J.; Bretonnière, Y.; Andraud, C. Neutral push-pull chromophores for nonlinear optical imaging of cell membranes. *Org. Biomol. Chem.* **2010**, *8*, 142–150. [[CrossRef](#)] [[PubMed](#)]
56. Axelrod, D.; Koppel, D.E.; Schlessinger, J.; Elson, E.; Webb, W.W. Mobility measurement by analysis of fluorescence photobleaching recovery kinetics. *Biophys. J.* **1976**, *16*, 1055–1069. [[CrossRef](#)]
57. Klymchenko, A.S. Solvatochromic and fluorogenic dyes as environment-sensitive probes: Design and biological applications. *Acc. Chem. Res.* **2017**, *50*, 366–375. [[CrossRef](#)] [[PubMed](#)]
58. Lee, M.H.; Kim, J.S.; Sessler, J.L. Small molecule-based ratiometric fluorescence probes for cations, anions, and biomolecules. *Chem. Soc. Rev.* **2015**, *44*, 4185–4191. [[CrossRef](#)] [[PubMed](#)]
59. Hildebrandt, N.; Spillmann, C.M.; Algar, W.R.; Pons, T.; Stewart, M.H.; Oh, E.; Susumu, K.; Díaz, S.A.; Delehanty, J.B.; Medintz, I.L. Energy transfer with semiconductor quantum dot bioconjugates: A versatile platform for biosensing, energy harvesting, and other developing applications. *Chem. Rev.* **2017**, *117*, 536–711. [[CrossRef](#)] [[PubMed](#)]
60. Shimomura, O.; Johnson, F.H.; Saiga, Y. Extraction, purification and properties of aequorin, a bioluminescent protein from the luminous hydromedusan, Aequorea. *J. Cell. Comp. Physiol.* **1962**, *59*, 223–239. [[CrossRef](#)] [[PubMed](#)]
61. Shagin, D.A.; Barsova, E.V.; Yanushevich, Y.G.; Fradkov, A.F.; Lukyanov, K.A.; Labas, Y.A.; Semenova, T.N.; Ugalde, J.A.; Meyers, A.; Nunez, J.M.; et al. GFP-like proteins as ubiquitous metazoan superfamily: Evolution of functional features and structural complexity. *Mol. Biol. Evol.* **2004**, *21*, 841–850. [[CrossRef](#)] [[PubMed](#)]
62. Deheyn, D.D.; Kubokawa, K.; McCarthy, J.K.; Murakami, A.; Porrachia, M.; Rouse, G.W.; Holland, N.D. Endogenous green fluorescent protein (GFP) in amphioxus. *Biol. Bull.* **2007**, *213*, 95–100. [[CrossRef](#)] [[PubMed](#)]
63. Shcherbakova, D.M.; Subach, O.M.; Verkhusha, V.V. Red fluorescent proteins: Advanced imaging applications and future design. *Angew. Chem. Int. Ed. Engl.* **2012**, *51*, 10724–10738. [[CrossRef](#)] [[PubMed](#)]
64. Cranfill, P.J.; Sell, B.R.; Baird, M.A.; Allen, J.R.; Lavagnino, Z.; Gruiter, H.M.; de Kremers, G.J.; Davidson, M.W.; Ustione, A.; Piston, D.W. Quantitative assessment of fluorescent proteins. *Nat. Methods* **2016**, *13*, 557–562. [[CrossRef](#)] [[PubMed](#)]
65. Shaner, N.C.; Campbell, R.E.; Steinbach, P.A.; Giepmans, B.N.; Palmer, A.E.; Tsien, R.Y. Improved monomeric red, orange and yellow fluorescent proteins derived from *Discosoma* sp. red fluorescent protein. *Nat. Biotechnol.* **2004**, *22*, 1567–1572. [[CrossRef](#)] [[PubMed](#)]
66. Shcherbo, D.; Merzlyak, E.M.; Chepurnykh, T.V.; Fradkov, A.F.; Ermakova, G.V.; Solovieva, E.A.; Lukyanov, K.A.; Bogdanova, E.A.; Zaraisky, A.G.; Lukyanov, S.; et al. Bright far-red fluorescent protein for whole-body imaging. *Nat. Methods* **2007**, *4*, 741–746. [[CrossRef](#)] [[PubMed](#)]
67. Shcherbo, D.; Murphy, C.S.; Ermakova, G.V.; Solovieva, E.A.; Chepurnykh, T.V.; Shcheglov, A.S.; Verkhusha, V.V.; Pletnev, V.Z.; Hazelwood, K.L.; Roche, P.M.; et al. Far-red fluorescent tags for protein imaging in living tissues. *Biochem. J.* **2009**, *418*, 567–574. [[CrossRef](#)] [[PubMed](#)]
68. Berezin, M.Y.; Achilefu, S. Fluorescence lifetime measurements and biological imaging. *Chem. Rev.* **2010**, *110*, 2641–2684. [[CrossRef](#)] [[PubMed](#)]
69. Becker, W. Fluorescence lifetime imaging—Techniques and applications. *J. Microsc.* **2012**, *247*, 119–136. [[CrossRef](#)] [[PubMed](#)]
70. Chen, L.C.; Lloyd, W.R.; Chang, C.W.; Sud, D.; Mycek, M.A. Fluorescence lifetime imaging microscopy for quantitative biological imaging. *Methods Cell Biol.* **2013**, *114*, 457–488. [[PubMed](#)]
71. Suhling, K.W.; French, P.M.; Phillips, D. Time-resolved fluorescence microscopy. *Photochem. Photobiol. Sci.* **2005**, *4*, 13–22. [[CrossRef](#)] [[PubMed](#)]
72. Suhling, K.; Hirvonen, L.M.; Levitt, J.A.; Chung, P.H.; Tregidgo, C.; Le Marois, A.; Rusakov, D.A.; Zheng, K.; Ameer-Beg, S.; Poland, S.; et al. Fluorescence lifetime imaging (FLIM): Basic concepts and some recent developments. *Med. Photonics* **2015**, *27*, 3–40. [[CrossRef](#)]
73. Sailer, B.L.; Valdez, J.G.; Steinkamp, J.A.; Crissman, H.A. Apoptosis induced with different cycle-perturbing agents produces differential changes in the fluorescence lifetime of DNA-bound ethidium bromide. *Cytometry* **1998**, *31*, 208–216. [[CrossRef](#)]
74. Cubeddu, R.; Canti, G.; Taroni, P.; Valentini, G. Time-gated fluorescence imaging for the diagnosis of tumors in a murine model. *Photochem. Photobiol.* **1993**, *57*, 480–485. [[CrossRef](#)] [[PubMed](#)]

75. Picot, A.; D'Aléo, A.; Baldeck, P.L.; Grichine, A.; Duperray, A.; Andraud, C.; Maury, O. Long-lived two-photon excited luminescence of water-soluble europium complex: Applications in biological imaging using two-photon scanning microscopy. *J. Am. Chem. Soc.* **2008**, *130*, 1532–1533. [[CrossRef](#)] [[PubMed](#)]
76. Yang, C.J.; Jockusch, S.; Vicens, M.; Turro, N.J.; Tan, W. Light-switching excimer probes for rapid protein monitoring in complex biological fluids. *Proc. Natl. Acad. Sci. USA* **2005**, *102*, 17278–17283. [[CrossRef](#)] [[PubMed](#)]
77. Lu, Y.; Zhao, J.; Zhang, R.; Liu, Y.; Liu, D.; Goldys, E.M.; Yang, X.; Xi, P.; Sunna, A.; Lu, J.; et al. Tunable lifetime multiplexing using luminescent nanocrystals. *Nat. Photonics* **2014**, *8*, 32–36. [[CrossRef](#)]
78. Zhong, W.; Urayama, P.; Mycek, M.A. Imaging fluorescence lifetime modulation of a ruthenium-based dye in living cells: The potential for oxygen sensing. *J. Phys. D Appl. Phys.* **2003**, *36*, 1689. [[CrossRef](#)]
79. Gerritsen, H.C.; Sanders, R.; Draaijer, A.; Ince, C.; Levine, Y.K. Fluorescence lifetime imaging of oxygen in living cells. *J. Fluoresc.* **1997**, *7*, 11–15. [[CrossRef](#)]
80. Gatzogiannis, E.; Chen, Z.; Wei, L.; Wombacher, R.; Kao, Y.T.; Yefremov, G.; Cornish, V.W.; Min, W. Mapping protein-specific micro-environments in live cells by fluorescence lifetime imaging of a hybrid genetic-chemical molecular rotor tag. *Chem. Commun.* **2012**, *48*, 8694–8696. [[CrossRef](#)] [[PubMed](#)]
81. Carlsson, K.; Liljeborg, A.; Andersson, R.M.; Brismar, H. Confocal pH imaging of microscopic specimens using fluorescence lifetimes and phase fluorometry: Influence of parameter choice on system performance. *J. Microsc.* **2000**, *199*, 106–114. [[CrossRef](#)] [[PubMed](#)]
82. Hanson, K.M.; Behne, M.J.; Barry, N.P.; Mauro, T.M.; Gratton, E.; Clegg, R.M. Two-photon fluorescence lifetime imaging of the skin stratum corneum pH gradient. *Biophys. J.* **2002**, *83*, 1682–1690. [[CrossRef](#)]
83. Bajar, B.T.; Wang, E.S.; Zhang, S.; Lin, M.Z.; Chu, J. A guide to fluorescent protein FRET pairs. *Sensors* **2016**, *16*, E1488. [[CrossRef](#)] [[PubMed](#)]
84. Pawlicki, M.; Collins, H.A.; Denning, R.G.; Anderson, H.L. Two-photon absorption and the design of two-photon dyes. *Angew. Chem. Int. Ed.* **2009**, *48*, 3244–3266. [[CrossRef](#)] [[PubMed](#)]
85. He, G.S.; Tan, L.S.; Zheng, Q.; Prasad, P.N. Multiphoton absorbing materials: Molecular designs, characterizations, and applications. *Chem. Rev.* **2008**, *108*, 1245–1330. [[CrossRef](#)] [[PubMed](#)]
86. Denk, W.; Strickler, J.H.; Webb, W.W. Two-photon laser scanning fluorescence microscopy. *Science* **1990**, *248*, 73–76. [[CrossRef](#)] [[PubMed](#)]
87. Helmchen, F.; Denk, W. Deep tissue two-photon microscopy. *Nat. Methods* **2005**, *2*, 932–940. [[CrossRef](#)] [[PubMed](#)]
88. Kim, D.; Ryu, H.G.; Ahn, K.H. Recent development of two-photon fluorescent probes for bioimaging. *Org. Biomol. Chem.* **2014**, *12*, 4550–4566. [[CrossRef](#)] [[PubMed](#)]
89. Kim, H.M.; Cho, B.R. Small-molecule two-photon probes for bioimaging applications. *Chem. Rev.* **2015**, *115*, 5014–5055. [[CrossRef](#)] [[PubMed](#)]
90. Rumi, M.; Ehrlich, J.E.; Heikal, A.A.; Perry, J.W.; Barlow, S.; Hu, Z.; McCord-Maughon, D.; Parker, T.C.; Röckel, H.; Thayumanavan, S. Structure–property relationships for two-photon absorbing chromophores: Bis-donor diphenylpolyene and bis(styryl)benzene derivatives. *J. Am. Chem. Soc.* **2000**, *122*, 9500–9510. [[CrossRef](#)]
91. Drobizhev, M.; Makarov, N.S.; Tillo, S.E.; Hughes, T.E.; Rebane, A. Two-photon absorption properties of fluorescent proteins. *Nat. Methods* **2011**, *8*, 393–399. [[CrossRef](#)] [[PubMed](#)]
92. Molina, R.S.; Tran, T.M.; Campbell, R.E.; Lambert, G.G.; Salih, A.; Shaner, N.C.; Hughes, T.E.; Drobizhev, M. Blue-shifted green fluorescent protein homologues are brighter than enhanced Green Fluorescent Protein under two-photon excitation. *J. Phys. Chem. Lett.* **2017**, *8*, 2548–2554. [[CrossRef](#)] [[PubMed](#)]
93. Hell, S.W. Far-field optical nanoscopy. *Science* **2007**, *316*, 1153–1158. [[CrossRef](#)] [[PubMed](#)]
94. Müller, T.; Schumann, C.; Kraegeloh, A. STED microscopy and its applications: New insights into cellular processes on the nanoscale. *Chem. Phys. Chem.* **2012**, *13*, 1986–2000. [[CrossRef](#)] [[PubMed](#)]
95. Eggeling, C.; Willig, K.I.; Barrantes, F.J. STED microscopy of living cells—New frontiers in membrane and neurobiology. *J. Neurochem.* **2013**, *126*, 203–212. [[CrossRef](#)] [[PubMed](#)]
96. Sednev, M.V.; Belov, V.N.; Hell, S.W. Fluorescent dyes with large Stokes shifts for super-resolution optical microscopy of biological objects: A review. *Methods Appl. Fluoresc.* **2015**, *3*, 042004. [[CrossRef](#)] [[PubMed](#)]
97. Hess, S.T.; Girirajan, T.P.K.; Mason, M.D. Ultra-high resolution imaging by fluorescence photoactivation localization microscopy. *Biophys. J.* **2006**, *91*, 4258–4272. [[CrossRef](#)] [[PubMed](#)]

98. Subach, F.V.; Patterson, G.H.; Manley, S.; Gillette, J.M.; Lippincott-Schwartz, J.; Verkhusha, V.V. Photoactivatable mCherry for high-resolution two-color fluorescence microscopy. *Nat. Methods* **2009**, *6*, 153–159. [[CrossRef](#)] [[PubMed](#)]
99. Schoen, I.; Ries, J.; Klotzsch, E.; Ewers, H.; Vogel, V. Binding-activated localization microscopy of DNA structures. *Nano Lett.* **2011**, *11*, 4008–4011. [[CrossRef](#)] [[PubMed](#)]
100. Rust, M.J.; Bates, M.; Zhuang, X. Sub-diffraction-limit imaging by stochastic optical reconstruction microscopy (STORM). *Nat. Methods* **2006**, *3*, 793–796. [[CrossRef](#)] [[PubMed](#)]
101. Bates, M.; Huang, B.; Dempsey, G.T.; Zhuang, X. Multicolor super-resolution imaging with photo-switchable fluorescent probes. *Science* **2007**, *317*, 1749–1753. [[CrossRef](#)] [[PubMed](#)]
102. Irie, M.; Fukaminato, T.; Matsuda, K.; Kobatake, S. Photochromism of diarylethene molecules and crystals: Memories, switches, and actuators. *Chem. Rev.* **2014**, *114*, 12174–12277. [[CrossRef](#)] [[PubMed](#)]
103. Nienhaus, K.; Nienhaus, G.U. Fluorescent proteins for live-cell imaging with super-resolution. *Chem. Soc. Rev.* **2014**, *43*, 1088–1106. [[CrossRef](#)] [[PubMed](#)]
104. Shcherbakova, D.M.; Sengupta, P.; Lippincott-Schwartz, J.; Verkhusha, V.V. Photocontrollable fluorescent proteins for superresolution imaging. *Annu. Rev. Biophys.* **2014**, *43*, 303–329. [[CrossRef](#)] [[PubMed](#)]
105. Yang, N.J.; Hinner, M.J. Getting across the cell membrane: An overview for small molecules, peptides, and proteins. *Methods Mol. Biol.* **2015**, *1266*, 29–53. [[PubMed](#)]
106. Mobbs, P.; Becker, D.; Williamson, R.; Bate, M.; Warner, A. Techniques for dye injection and cell labeling. In *Microelectrode Techniques, The Plymouth Workshop Handbook*, 2nd ed.; Ogden, D.C., Ed.; The Company of Biologists Ltd.: Cambridge, UK, 1994; pp. 361–387.
107. Strouse, J.J.; Ivnitiski-Steele, I.; Waller, A.; Young, S.M.; Perez, D.; Evangelisti, A.M.; Ursu, O.; Bologa, C.G.; Carter, M.B.; Salas, V.M.; et al. Fluorescent substrates for flow cytometric evaluation of efflux inhibition in ABCB1, ABCC1, and ABCG2 transporters. *Anal. Biochem.* **2013**, *437*, 77–87. [[CrossRef](#)] [[PubMed](#)]
108. Jobsis, P.D.; Rothstein, E.C.; Balaban, R.S. Limited utility of acetoxymethyl (AM)-based intracellular delivery systems, in vivo: Interference by extracellular esterases. *J. Microsc.* **2007**, *226*, 74–81. [[CrossRef](#)] [[PubMed](#)]
109. Bozyczko-Coyne, D.; McKenna, B.W.; Connors, T.J.; Neff, N.T. A rapid fluorometric assay to measure neuronal survival in vitro. *J. Neurosci. Methods* **1993**, *50*, 205–216. [[CrossRef](#)]
110. Vaudry, D.; Rousselle, C.; Basille, M.; Falluel-Morel, A.; Pamantung, T.F.; Fontaine, M.; Fournier, A.; Vaudry, H.; Gonzalez, B.J. Pituitary adenylate cyclase-activating polypeptide protects rat cerebellar granule neurons against ethanol-induced apoptotic cell death. *Proc. Natl. Acad. Sci. USA* **2002**, *99*, 6398–6403. [[CrossRef](#)] [[PubMed](#)]
111. Raoult, E.; Bénard, M.; Komuro, H.; Lebon, A.; Vivien, D.; Fournier, A.; Vaudry, H.; Vaudry, D.; Galas, L. Cortical-layer-specific effects of PACAP and tPA on interneuron migration during post-natal development of the cerebellum. *J. Neurochem.* **2014**, *130*, 241–254. [[CrossRef](#)] [[PubMed](#)]
112. Uenishi, E.; Shibasaki, T.; Takahashi, H.; Seki, C.; Hamaguchi, H.; Yasuda, T.; Tatebe, M.; Oiso, Y.; Takenawa, T.; Seino, S. Actin dynamics regulated by the balance of neuronal Wiskott-Aldrich Syndrome Protein (N-WASP) and cofilin activities determines the biphasic response of glucose-induced insulin secretion. *J. Biol. Chem.* **2013**, *288*, 25851–25864. [[CrossRef](#)] [[PubMed](#)]
113. Schapman, D.; Perraudau, C.; Bénard, M.; Gallarvardin, T.; Boulangé, A.; Leleu, S.; Lebon, A.; Franck, X.; Galas, L. Characterization of fluorescent synthetic epicocconone-based dye through advanced light microscopies for live cell imaging applications. *Dyes Pigment.* **2017**, *141*, 394–405. [[CrossRef](#)]
114. Pasquier, J.; Galas, L.; Boulangé-Lecomte, C.; Rioult, D.; Bultelle, F.; Magal, P.; Webb, G.; Le Foll, F. Different modalities of intercellular membrane exchanges mediate cell-to-cell p-glycoprotein transfers in MCF-7 breast cancer cells. *J. Biol. Chem.* **2012**, *287*, 7374–7387. [[CrossRef](#)] [[PubMed](#)]
115. Bantly, A.D.; Gray, B.D.; Breslin, E.; Weinstein, E.G.; Muirhead, K.A.; Ohlsson-Wilhelm, B.M.; Moore, J.S. CellVue Claret, a new far-red dye, facilitates polychromatic assessment of immune cell proliferation. *Immunol. Invest.* **2007**, *36*, 581–605. [[CrossRef](#)] [[PubMed](#)]
116. Beem, E.; Segal, M.S. Evaluation of stability and sensitivity of cell fluorescent labels when used for cell migration. *J. Fluoresc.* **2013**, *23*, 975–987. [[CrossRef](#)] [[PubMed](#)]
117. Takeshita, Y.; Obermeier, B.; Coteleur, A.; Sano, Y.; Kanda, T.; Ransohoff, R.M. An in vitro blood-brain barrier model combining shear stress and endothelial cell/astrocyte co-culture. *J. Neurosci. Methods* **2014**, *232*, 165. [[CrossRef](#)] [[PubMed](#)]

118. Hendrickson, O.D.; Zherdev, A.V. Analytical application of lectins. *Crit. Rev. Anal. Chem.* **2018**, *48*, 279–292. [[CrossRef](#)] [[PubMed](#)]
119. Monsigny, M.; Roche, A.C.; Sene, C.; Maget-Dana, R.; Delmotte, F. Sugar-lectin interactions: How does wheat-germ agglutinin bind sialoglycoconjugates? *Eur. J. Biochem.* **1979**, *104*, 147–153. [[CrossRef](#)]
120. Panchuk-Voloshina, N.; Haugland, R.P.; Bishop-Stewart, J.; Bhalgat, M.K.; Millard, P.J.; Mao, F.; Leung, W.Y.; Haugland, R.P. Alexa dyes, a series of new fluorescent dyes that yield exceptionally bright, photostable conjugates. *J. Histochem. Cytochem.* **1999**, *47*, 1179–1188. [[CrossRef](#)] [[PubMed](#)]
121. Berlier, J.E.; Rothe, A.; Buller, G.; Bradford, J.; Gray, D.R.; Filanoski, B.J.; Telford, W.G.; Yue, S.; Liu, J.; Cheung, C.Y.; et al. Quantitative comparison of long-wavelength Alexa Fluor dyes to Cy dyes: Fluorescence of the dyes and their bioconjugates. *J. Histochem. Cytochem.* **2003**, *51*, 1699–1712. [[CrossRef](#)] [[PubMed](#)]
122. Bénard, M.; Schapman, D.; Lebon, A.; Monterroso, B.; Bellenger, M.; Le Foll, F.; Pasquier, J.; Vaudry, H.; Vaudry, D.; Galas, L. Structural and functional analysis of tunneling nanotubes (TnTs) using gCW STED and gconfocal approaches. *Biol. Cell* **2015**, *107*, 419–425. [[CrossRef](#)] [[PubMed](#)]
123. Latt, S.A.; Stetten, G.; Juergens, L.A.; Willard, H.F.; Scher, C.D. Recent developments in the detection of deoxyribonucleic acid synthesis by 33258 Hoechst fluorescence. *J. Histochem. Cytochem.* **1975**, *23*, 493–505. [[CrossRef](#)] [[PubMed](#)]
124. Bucevicius, J.; Lukinavičius, G.; Gerassimaitė, R. The use of Hoeschst dyes for DNA staining and beyond. *Chemosensors* **2018**, *6*, 18. [[CrossRef](#)]
125. Pasquier, J.; Guerrouahen, B.S.; Al Thawadi, H.; Ghiabi, P.; Maleki, M.; Abu-Kaoud, N.; Jacob, A.; Mirshahi, M.; Galas, L.; Rafii, S.; et al. Preferential transfer of mitochondria from endothelial to cancer cells through tunneling nanotubes modulates chemoresistance. *J. Transl. Med.* **2013**, *11*, 94. [[CrossRef](#)] [[PubMed](#)]
126. Caicedo, A.; Fritz, V.; Brondello, J.M.; Ayala, M.; Dennemont, I.; Abdellaoui, N.; de Fraipont, F.; Moisan, A.; Prouteau, C.A.; Boukhaddaoui, H.; et al. MitoCeption as a new tool to assess the effects of mesenchymal stem/stromal cell mitochondria on cancer cell metabolism and function. *Sci. Rep.* **2015**, *5*, 9073. [[CrossRef](#)] [[PubMed](#)]
127. Nzigou Mombo, B.; Gerbal-Chaloin, S.; Bokus, A.; Daujat-Chavanieu, M.; Jorgensen, C.; Hugnot, J.P.; Vignais, M.L. MitoCeption: Transferring isolated human MSC mitochondria to glioblastoma stem cells. *J. Vis. Exp.* **2017**, *120*, e55245. [[CrossRef](#)] [[PubMed](#)]
128. Haugland, R.P. *The Handbook: A Guide to Fluorescent Probes and Labeling Technologies*, 10th ed.; Molecular Probes, Invitrogen Corp.: Carlsbad, CA, USA, 2005; p. 1126, ISBN 978-0971063648.
129. Han, Y.; Li, M.; Qiu, F.; Zhang, M.; Zhang, Y.H. Cell-permeable organic fluorescent probes for live-cell long-term super-resolution imaging reveal lysosome-mitochondrion interactions. *Nat. Commun.* **2017**, *8*, 1307. [[CrossRef](#)] [[PubMed](#)]
130. McCann, T.E.; Kosaka, N.; Koide, Y.; Mitsunaga, M.; Choyke, P.L.; Nagano, T.; Urano, Y.; Kobayashi, H. Activatable optical imaging with a silica-rhodamine based near infrared (SiR700) fluorophore: A comparison with cyanine based dyes. *Bioconjug. Chem.* **2011**, *22*, 2531–2538. [[CrossRef](#)] [[PubMed](#)]
131. Lukinavičius, G.; Umezawa, K.; Olivier, N.; Honigsmann, A.; Yang, G.; Plass, T.; Mueller, V.; Reymond, L.; Corrêa, I.R., Jr.; Luo, Z.G.; et al. Near-infrared fluorophore for live-cell super-resolution microscopy of cellular proteins. *Nat. Chem.* **2013**, *5*, 132–139. [[CrossRef](#)] [[PubMed](#)]
132. Fong, M.; Lesnik, J.; Li, G.; Antes, T.J.; Lu, B. Cyto-Tracers™: Novel lentiviral-based molecular imaging tools. *Biotechniques* **2018**, *49*, 5. [[CrossRef](#)]
133. Baskin, J.M.; Prescher, J.A.; Laughlin, S.T.; Agard, N.J.; Chang, P.V.; Miller, I.A.; Lo, A.; Codelli, J.A.; Bertozzi, C.R. Copper-free click chemistry for dynamic in vivo imaging. *Proc. Natl. Acad. Sci. USA* **2007**, *104*, 16793–16797. [[CrossRef](#)] [[PubMed](#)]
134. Niederwieser, A.; Späte, A.K.; Nguyen, L.D.; Jüngst, C.; Reutter, W.; Wittmann, V. Two-color glycan labeling of live cells by a combination of Diels–Alder and click chemistry. *Angew. Chem. Int. Ed.* **2013**, *52*, 4265–4268. [[CrossRef](#)] [[PubMed](#)]
135. Dumont, M.; Lehner, A.; Vauzeilles, B.; Malassis, J.; Marchant, A.; Smyth, K.; Linclau, B.; Baron, A.; Mas Pons, J.; Anderson, C.T.; et al. Plant cell wall imaging by metabolic click-mediated labelling of rhamnogalacturonan II using azido 3-deoxy-d-manno-oct-2-ulosonic acid. *Plant J.* **2016**, *85*, 437–447. [[CrossRef](#)] [[PubMed](#)]
136. Chang, P.V.; Chen, X.; Smyrniotis, C.; Xenakis, A.; Hu, T.; Bertozzi, C.R.; Wu, P. Metabolic labeling of sialic acids in living animals with alkynyl sugars. *Angew. Chem. Int. Ed.* **2009**, *48*, 4030–4033. [[CrossRef](#)] [[PubMed](#)]

137. Hoogenboom, J.; Berghuis, N.; Cramer, D.; Geurts, R.; Zuilhof, H.; Wennekes, T. Direct imaging of glycans in Arabidopsis roots via click labeling of metabolically incorporated azido-monosaccharides. *BMC Plant Biol.* **2016**, *16*, 220. [[CrossRef](#)] [[PubMed](#)]
138. García-Plazaola, J.I.; Fernández-Marín, B.; Duke, S.; Hernández, A.; López-Arbeloa, F.; Becerril, J.M. Autofluorescence: Biological functions and technical applications. *Plant. Sci.* **2015**, *236*, 136–145. [[CrossRef](#)] [[PubMed](#)]
139. Millie, D.; Schofield, O.; Kirkpatrick, G.; Johnsen, G.; Evens, T. Using absorbance and fluorescence spectra to discriminate microalgae. *Eur. J. Phycol.* **2002**, *37*, 313–322. [[CrossRef](#)]
140. Elias, S.; Delestre, C.; Ory, S.; Marais, S.; Courel, M.; Vazquez-Martinez, R.; Bernard, S.; Coquet, L.; Malagon, M.M.; Driouich, A.; et al. Chromogranin A induces the biogenesis of granules with calcium- and actin-dependent dynamics and exocytosis in constitutively secreting cells. *Endocrinology* **2012**, *153*, 4444–4456. [[CrossRef](#)] [[PubMed](#)]
141. Kube, S.; Hersch, N.; Naumovska, E.; Gensch, T.; Hendriks, J.; Franzen, A.; Landvogt, L.; Siebrasse, J.P.; Kubitscheck, U.; Hoffmann, B.; et al. Fusogenic Liposomes as nanocarriers for the delivery of intracellular proteins. *Langmuir* **2017**, *33*, 1051–1059. [[CrossRef](#)] [[PubMed](#)]
142. Griffin, B.A.; Adams, S.R.; Tsien, R.Y. Specific covalent labeling of recombinant protein molecules inside live cells. *Science* **1998**, *281*, 269–272. [[CrossRef](#)] [[PubMed](#)]
143. Keppler, A.; Gendreizig, S.; Gronemeyer, T.; Pick, H.; Vogel, H.; Johnsson, K. A general method for the covalent labeling of fusion proteins with small molecules in vivo. *Nat. Biotechnol.* **2003**, *21*, 86–89. [[CrossRef](#)] [[PubMed](#)]
144. Gautier, A.; Juillerat, A.; Heinis, C.; Corrêa, I.R., Jr.; Kindermann, M.; Beaufils, F.; Johnsson, K. An engineered protein tag for multiprotein labeling in living cells. *Chem. Biol.* **2008**, *15*, 128–136. [[CrossRef](#)] [[PubMed](#)]
145. Los, G.V.; Darzins, A.; Karassina, N.; Zimprinch, C.; Learish, R.; McDougall, M.G.; Encell, L.P.; Friedman-Ohana, R.; Wood, M.; Vidurgiris, G.; et al. HaloTagTM interchangeable labeling technology for cell imaging and protein capture. *Promega Cell Notes* **2005**, *11*, 2–6.
146. Crivat, G.; Taraska, J.W. Imaging proteins inside cells with fluorescent tags. *Trends Biotechnol.* **2012**, *30*, 8–16. [[CrossRef](#)] [[PubMed](#)]
147. Martin, B.R.; Giepmans, B.N.; Adams, S.R.; Tsien, R.Y. Mammalian cell-based optimization of the biarsenical-binding tetracysteine motif for improved fluorescence and affinity. *Nat. Biotechnol.* **2005**, *23*, 1308–1314. [[CrossRef](#)] [[PubMed](#)]
148. Bosch, P.J.; Corrêa, I.R., Jr.; Sonntag, M.H.; Ibach, J.; Brunsveld, L.; Kanger, J.S.; Subramaniam, V. Evaluation of fluorophores to label SNAP-tag fused proteins for multicolor single-molecule tracking microscopy in live cells. *Biophys. J.* **2014**, *107*, 803–814. [[CrossRef](#)] [[PubMed](#)]
149. England, C.G.; Luo, H.; Cai, W. HaloTag technology: A versatile platform for biomedical applications. *Bioconjug. Chem.* **2015**, *26*, 975–986. [[CrossRef](#)] [[PubMed](#)]
150. Meng, X.; Liu, J.; Yu, X.; Li, J.; Lu, X.; Shen, T. Pluronic F127 and D- α -tocopheryl polyethylene glycol succinate (TPGS) mixed micelles for targeting drug delivery across the blood brain barrier. *Sci. Rep.* **2017**, *7*, 2964. [[CrossRef](#)] [[PubMed](#)]
151. Galas, L.; Lamacz, M.; Garnier, M.; Roubos, E.W.; Tonon, M.C.; Vaudry, H. Involvement of extracellular and intracellular calcium sources in TRH-induced α -MSH secretion from frog melanotrope cells. *Mol. Cell. Endocrinol.* **1998**, *138*, 25–39. [[CrossRef](#)]
152. Galas, L.; Garnier, M.; Lamacz, M. Calcium waves in frog melanotrophs are generated by intracellular inactivation of TTX-sensitive membrane Na⁺ channel. *Mol. Cell. Endocrinol.* **2000**, *170*, 197–209. [[CrossRef](#)]
153. Bénard, M.; Gonzalez, B.J.; Schouft, M.T.; Falluel-Morel, A.; Vaudry, D.; Chan, P.; Vaudry, H.; Fontaine, M. Characterization of C3a and C5a receptors in rat cerebellar granule neurons during maturation. Neuroprotective effect of C5a against apoptotic cell death. *J. Biol. Chem.* **2004**, *279*, 43487–43496. [[CrossRef](#)] [[PubMed](#)]
154. Gach, K.; Belkacemi, O.; Lefranc, B.; Perlikowski, P.; Masson, J.; Walet-Balieu, M.L.; Do-Rego, J.C.; Galas, L.; Schapman, D.; Lamtahri, R.; et al. Detection, characterization and biological activities of [bisphospho-thr3,9]ODN, an endogenous molecular form of ODN released by astrocytes. *Neuroscience* **2015**, *290*, 472–484. [[CrossRef](#)] [[PubMed](#)]
155. Qu, H.; Xing, W.; Wu, F.; Wang, Y. Rapid and inexpensive method of loading fluorescent dye into pollen tubes and root hairs. *PLoS ONE* **2016**, *11*, e0152320. [[CrossRef](#)] [[PubMed](#)]

156. Ona-Jodar, T.; Gerkau, N.J.; Sara Aghvami, S.; Rose, C.R.; Egger, V. Two-photon Na^+ imaging reports somatically evoked action potentials in rat olfactory bulb mitral and granule cell neurites. *Front. Cell. Neurosci.* **2017**, *11*, 50. [[CrossRef](#)] [[PubMed](#)]
157. Nejdli, L.; Moravanska, A.; Smerkova, K.; Mravec, F.; Krizkova, S.; Pomorski, A.; Krežel, A.; Macka, M.; Adam, V.; Vaculovicova, M. Short-sweep capillary electrophoresis with a selective zinc fluorescence imaging reagent FluoZin-3 for determination of free and metallothionein-2a-bound Zn^{2+} ions. *Anal. Chim. Acta.* **2018**, *1017*, 41–47. [[CrossRef](#)] [[PubMed](#)]
158. Suzuki, Y.; Komatsu, H.; Ikeda, T.; Saito, N.; Araki, S.; Citterio, D.; Hisamoto, D.; Kitamura, Y.; Kubota, T.; Nakagawa, J.; et al. Design and synthesis of Mg^{2+} -selective fluoroionophores based on a coumarin derivative and application for Mg^{2+} measurement in a living cell. *Anal. Chem.* **2002**, *74*, 1423–1428. [[CrossRef](#)] [[PubMed](#)]
159. Falluel-Morel, A.; Aubert, N.; Vaudry, D.; Basille, M.; Fontaine, M.; Fournier, A.; Vaudry, H.; Gonzalez, B.J. Opposite regulation of the mitochondrial apoptotic pathway by C2-ceramide and PACAP through a MAP-kinase-dependent mechanism in cerebellar granule cells. *J. Neurochem.* **2004**, *91*, 1231–1243. [[CrossRef](#)] [[PubMed](#)]
160. Zahid, A.; Despres, J.; Bénard, M.; Nguema-Ona, E.; Leprince, J.; Vaudry, D.; Rihouey, C.; Vicré-Gibouin, M.; Driouich, A.; Follet-Gueye, M.L. Arabinogalactan Proteins from Baobab and Acacia Seeds Influence Innate Immunity of Human Keratinocytes in vitro. *J. Cell. Physiol.* **2017**, *232*, 2558–2568. [[CrossRef](#)] [[PubMed](#)]
161. Chennoufi, R.; Bougherara, H.; Gagey-Eilstein, N.; Dumat, B.; Henry, E.; Subra, F.; Bury-Moné, S.; Mahuteau-Betzer, F.; Tauc, P.; Teulade-Fichou, M.P.; et al. Mitochondria-targeted triphenylamine derivatives activatable by two-photon excitation for triggering and imaging cell apoptosis. *Sci. Rep.* **2016**, *6*, 21458. [[CrossRef](#)] [[PubMed](#)]
162. Bortolozzi, R.; von Gradowski, S.; Ihmels, H.; Schäfer, K.; Viola, G. Selective ratiometric detection of H_2O_2 in water and in living cells with boronobenzo[b]quinolizinium derivatives. *Chem. Commun.* **2014**, *50*, 8242–8245. [[CrossRef](#)] [[PubMed](#)]
163. Huo, Y.; Miao, J.; Han, L.; Li, Y.; Li, Z.; Shi, Y.; Guo, W. Selective and sensitive visualization of endogenous nitric oxide in living cells and animals by a Si-rhodamine deoxylactam-based near-infrared fluorescent probe. *Chem. Sci.* **2017**, *8*, 6857–6864. [[CrossRef](#)] [[PubMed](#)]
164. Hayashi, T.; Fukuda, N.; Uchiyama, S.; Inada, N. A cell-permeable fluorescent polymeric thermometer for intracellular temperature mapping in mammalian cell lines. *PLoS ONE* **2015**, *10*, e0117677. [[CrossRef](#)] [[PubMed](#)]
165. Figueroa, J.A.; Vignesh, K.S.; Deepe, G.S., Jr.; Caruso, J. Selectivity and specificity of small molecule fluorescent dyes/probes used for the detection of Zn^{2+} and Ca^{2+} in cells. *Metallomics* **2014**, *6*, 301–315. [[CrossRef](#)] [[PubMed](#)]
166. Chen, Z.; Truong, T.M.; Ai, H.-W. Illuminating brain activities with fluorescent protein-based biosensors. *Chemosensors* **2017**, *5*, 32. [[CrossRef](#)] [[PubMed](#)]
167. Bertolin, G.; Sizaire, F.; Herbomel, G.; Rebutier, D.; Prigent, C.; Tramier, M. A FRET biosensor reveals spatiotemporal activation and functions of aurora kinase A in living cells. *Nat. Commun.* **2016**, *7*, 12674. [[CrossRef](#)] [[PubMed](#)]
168. Miyawaki, A. Development of probes for cellular functions using fluorescent proteins and fluorescence resonance energy transfer. *Annu. Rev. Biochem.* **2011**, *80*, 357–373. [[CrossRef](#)] [[PubMed](#)]
169. Demeautis, C.; Sipietier, F.; Roul, J.; Chapuis, C.; Padilla-Parra, S.; Riquet, F.B.; Tramier, M. Multiplexing PKA and ERK1&2 kinases FRET biosensors in living cells using single excitation wavelength dual colour FLIM. *Sci. Rep.* **2017**, *7*, 41026. [[PubMed](#)]
170. Martin, K.J.; McGhee, E.J.; Schwarz, J.P.; Drysdale, M.; Brachmann, S.M.; Stucke, V.; Sansom, O.J.; Anderson, K.I. Accepting from the best donor; analysis of long-lifetime donor fluorescent protein pairings to optimise dynamic FLIM-based FRET experiments. *PLoS ONE* **2018**, *13*, e0183585. [[CrossRef](#)] [[PubMed](#)]
171. Franck, C.M.; Westermann, J.; Boisson-Dernier, A. Imaging Ca^{2+} dynamics in wild-type and NADPH oxidase-deficient mutant pollen tubes with yellow cameleon and confocal laser scanning microscopy. *Methods Mol. Biol.* **2017**, *1669*, 103–116. [[PubMed](#)]
172. Jazi, A.A.; Ploetz, E.; Arizki, M.; Dhandayuthapani, B.; Wacławska, I.; Krämer, R.; Ziegler, C.; Cordes, T. Caging and photoactivation in single-Molecule Förster Resonance Energy Transfer experiments. *Biochemistry.* **2017**, *56*, 2031–2041. [[CrossRef](#)] [[PubMed](#)]

173. FitzHarris, G. Monitoring microtubule dynamics in the mouse egg using photoactivatable-GFP-tubulin. *Methods Mol. Biol.* **2018**, *1818*, 137–144. [[PubMed](#)]
174. Dyer, L.A.; Patterson, C. A novel ex vivo culture method for the embryonic mouse heart. *J. Vis. Exp.* **2013**, *75*, e50359. [[CrossRef](#)] [[PubMed](#)]
175. Dailey, M.E.; Eyo, U.; Hass, J.; Kurpius, D. Imaging microglia in brain slices and slice cultures. *Cold Spring Harb. Protoc.* **2013**. [[CrossRef](#)] [[PubMed](#)]
176. Owusu-Ansah, E.; Yavari, A.; Banerjee, U. A protocol for in vivo detection of reactive oxygen species. *Protocol Exch.* **2008**. [[CrossRef](#)]
177. Cameron, D.B.; Galas, L.; Jiang, Y.; Raoult, E.; Vaudry, D.; Komuro, H. Cerebellar cortical-layer-specific control of neuronal migration by pituitary adenylate cyclase-activating polypeptide. *Neuroscience* **2007**, *146*, 697–712. [[CrossRef](#)] [[PubMed](#)]
178. Fahrion, J.K.; Komuro, Y.; Li, Y.; Ohno, N.; Littner, Y.; Raoult, E.; Galas, L.; Vaudry, D.; Komuro, H. Rescue of neuronal migration deficits in a mouse model of fetal Minamata disease by increasing neuronal Ca^{2+} spike frequency. *Proc. Natl. Acad. Sci. USA* **2012**, *109*, 5057–5062. [[CrossRef](#)] [[PubMed](#)]
179. Rakymzhan, A.; Radbruch, H.; Niesner, R.A. Quantitative imaging of Ca^{2+} by 3D-FLIM in live tissues. *Adv. Exp. Med. Biol.* **2017**, *1035*, 135–141. [[PubMed](#)]
180. Cameron, D.B.; Kasai, K.; Jiang, Y.; Hu, T.; Saeki, Y.; Komuro, H. Four distinct phases of basket/stellate cell migration after entering their final destination (the molecular layer) in the developing cerebellum. *Dev. Biol.* **2009**, *332*, 309–324. [[CrossRef](#)] [[PubMed](#)]
181. Mironov, S.L.; Skorova, E.; Taschenberger, G.; Hartelt, N.; Nikolaev, V.O.; Lohse, M.J.; Kügler, S. Imaging cytoplasmic cAMP in mouse brainstem neurons. *BMC Neurosci.* **2009**, *10*, 29. [[CrossRef](#)] [[PubMed](#)]
182. Uesaka, N.; Nishiwaki, M.; Yamamoto, N. Single cell electroporation method for axon tracing in cultured slices. *Dev. Growth Differ.* **2008**, *50*, 475–477. [[CrossRef](#)] [[PubMed](#)]
183. Henri, O.; Pouehe, C.; Houssari, M.; Galas, L.; Nicol, L.; Edwards-Lévy, F.; Henry, J.P.; Dumesnil, A.; Boukhalfa, I.; Banquet, S.; et al. Selective Stimulation of Cardiac Lymphangiogenesis Reduces Myocardial Edema and Fibrosis Leading to Improved Cardiac Function Following Myocardial Infarction. *Circulation* **2016**, *133*, 1484–1497. [[CrossRef](#)] [[PubMed](#)]
184. Pak, Y.L.; Swamy, K.M.; Yoon, J. Recent progress in fluorescent imaging probes. *Sensors* **2015**, *15*, 24374–24396. [[CrossRef](#)] [[PubMed](#)]
185. Icha, J.; Schmied, C.; Sidhaye, J.; Tomancak, P.; Preibisch, S.; Norden, C. Using light sheet fluorescence microscopy to image zebrafish eye development. *J. Vis. Exp.* **2016**, *110*, e53966. [[CrossRef](#)] [[PubMed](#)]
186. Levy, S.L.; White, J.J.; Lackey, E.P.; Schwartz, L.; Sillitoe, R.V. WGA-Alexa Conjugates for Axonal Tracing. *Curr. Protoc. Neurosci.* **2017**, *79*, 1–28. [[PubMed](#)]
187. Morishita, Y.; Kuroiwa, A.; Suzuki, T. Quantitative analysis of tissue deformation dynamics reveals three characteristic growth modes and globally aligned anisotropic tissue deformation during chick limb development. *Development* **2015**, *142*, 1672–1683. [[CrossRef](#)] [[PubMed](#)]
188. Porat-Shliom, N.; Chen, Y.; Tora, M.; Shitara, A.; Masedunskas, A.; Weigert, R. In vivo tissue-wide synchronization of mitochondrial metabolic oscillations. *Cell Rep.* **2014**, *9*, 514–521. [[CrossRef](#)] [[PubMed](#)]
189. Terai, T.; Nagano, T. Small-molecule fluorophores and fluorescent probes for bioimaging. *Pflugers Arch.* **2013**, *465*, 347–359. [[CrossRef](#)] [[PubMed](#)]
190. Tury, A.; Mairé-Coello, G.; DiCicco-Bloom, E. The cyclin-dependent kinase inhibitor p57Kip2 regulates cell cycle exit, differentiation, and migration of embryonic cerebral cortical precursors. *Cereb. Cortex* **2011**, *21*, 1840–1856. [[CrossRef](#)] [[PubMed](#)]
191. Mehrotra, P. Biosensors and their applications—A review. *J. Oral Biol. Craniofac. Res.* **2016**, *6*, 153–159. [[CrossRef](#)] [[PubMed](#)]
192. Brudno, Y.; Desai, R.M.; Kwee, B.J.; Joshi, N.S.; Aizenberg, M.; Mooney, D.J. In vivo targeting through click chemistry. *ChemMedChem* **2015**, *10*, 617–620. [[CrossRef](#)] [[PubMed](#)]
193. Kharkar, P.M.; Rehmann, M.S.; Skeens, K.M.; Maverakis, E.; Kloxin, A.M. Thiol-ene click hydrogels for therapeutic delivery. *ACS Biomater. Sci. Eng.* **2016**, *2*, 165–179. [[CrossRef](#)] [[PubMed](#)]
194. Smeets, N.M.; Bakaic, E.; Patenaude, M.; Hoare, T. Injectable poly(oligoethylene glycol methacrylate)-based hydrogels with tunable phase transition behaviours: Physicochemical and biological responses. *Acta Biomater.* **2014**, *10*, 4143–4155. [[CrossRef](#)] [[PubMed](#)]

195. O'Shea, T.M.; Aimetti, A.A.; Kim, E.; Yesilyurt, V.; Langer, R. Synthesis and characterization of a library of in-situ curing, nonswelling ethoxylated polyol thiol-ene hydrogels for tailorable macromolecule delivery. *Adv. Mater.* **2015**, *27*, 65–72. [[CrossRef](#)] [[PubMed](#)]
196. Somerville, C.R.; Bauer, S.; Brininstool, G.; Facette, M.; Hamann, T.; Milne, J.; Osborne, E.; Paredes, A.; Persson, S.; Raab, T.; et al. Toward a systems approach to understanding plant cell walls. *Science* **2004**, *306*, 2206–2211. [[CrossRef](#)] [[PubMed](#)]
197. McClosky, D.D.; Wang, B.; Chen, G.; Anderson, C.T. The click-compatible sugar 6-deoxy-alkynyl glucose metabolically incorporates into Arabidopsis root hair tips and arrests their growth. *Phytochemistry* **2016**, *123*, 16–24. [[CrossRef](#)] [[PubMed](#)]
198. Bukowski, N.; Pandey, J.L.; Doyle, L.; Richard, T.L.; Anderson, C.T.; Zhu, Y. Development of a clickable designer monolignol for interrogation of lignification in plant cell walls. *Bioconjug. Chem.* **2014**, *25*, 2189–2196. [[CrossRef](#)] [[PubMed](#)]
199. Pandey, J.L.; Kiemle, S.N.; Richard, T.L.; Zhu, Y.; Cosgrove, D.J.; Anderson, C.T. Investigating biochemical and developmental dependencies of lignification with a click-compatible monolignol analog in Arabidopsis thaliana stems. *Front. Plant. Sci.* **2016**, *7*, 1309. [[CrossRef](#)] [[PubMed](#)]
200. Anderson, C.T.; Wallace, I.S.; Somerville, C.R. Metabolic click-labeling with a fucose analog reveals pectin delivery, architecture, and dynamics in Arabidopsis cell walls. *Proc. Natl. Acad. Sci. USA* **2012**, *109*, 1329–1334. [[CrossRef](#)] [[PubMed](#)]
201. Wang, B.; McClosky, D.D.; Anderson, C.T.; Chen, G. Synthesis of a suite of click-compatible sugar analogs for probing carbohydrate metabolism. *Carbohydr. Res.* **2016**, *433*, 54–62. [[CrossRef](#)] [[PubMed](#)]
202. Chang, P.V.; Prescher, J.A.; Sletten, E.M.; Baskin, J.M.; Miller, I.A.; Agard, N.J.; Lo, A.; Bertozzi, C.R. Copper-free click chemistry in living animals. *Proc. Natl. Acad. Sci. USA* **2010**, *107*, 1821–1826. [[CrossRef](#)] [[PubMed](#)]
203. Lavis, L.D.; Raines, R.T. Bright building blocks for chemical biology. *ACS Chem. Biol.* **2014**, *9*, 855–866. [[CrossRef](#)] [[PubMed](#)]
204. Lavis, L.D. Chemistry is dead. Long live chemistry. *Biochemistry* **2017**, *56*, 5165–5170. [[CrossRef](#)] [[PubMed](#)]
205. Umezawa, K.; Citterio, D.; Suzuki, K. New trends in near-infrared fluorophores for bioimaging. *Anal. Sci.* **2014**, *30*, 327–349. [[CrossRef](#)] [[PubMed](#)]
206. Kiyose, K.; Kojima, H.; Nagano, T. Functional near-infrared fluorescent probes. *Chem. Asian J.* **2008**, *3*, 506–515. [[CrossRef](#)]
207. Hong, G.; Antaris, A.L.; Dai, H. Near-infrared fluorophores for biomedical imaging. *Nat. Biomed. Eng.* **2017**, *1*, 0010. [[CrossRef](#)]
208. Duval, R.; Duplais, C. Fluorescent natural products as probes and tracers in biology. *Nat. Prod. Rep.* **2017**, *34*, 161–193. [[CrossRef](#)] [[PubMed](#)]
209. De Moliner, F.; Kielland, N.; Lavilla, R.; Vendrell, M. Modern synthetic avenues for the preparation of functional fluorophores. *Angew. Chem. Int. Ed.* **2017**, *56*, 3758–3769. [[CrossRef](#)] [[PubMed](#)]
210. Alford, R.; Simpson, H.M.; Duberman, J.; Hill, G.C.; Ogawa, M.; Regino, C.; Kobayashi, H.; Choyke, P.L. Toxicity of organic fluorophores used in molecular imaging: Literature review. *Mol. Imaging* **2009**, *8*. [[CrossRef](#)]
211. Taraska, J.W.; Puljung, M.C.; Zagotta, W.N. Short-distance probes for protein backbone structure based on energy transfer between bimane and transition metal ions. *Proc. Natl. Acad. Sci. USA* **2009**, *106*, 16227–16232. [[CrossRef](#)] [[PubMed](#)]
212. Kowada, T.; Maeda, H.; Kikuchi, K. BODIPY-based probes for the fluorescence imaging of biomolecules in living cells. *Chem. Soc. Rev.* **2015**, *44*, 4953–4972. [[CrossRef](#)] [[PubMed](#)]
213. Sun, W.; Guo, S.; Hu, C.; Fan, J.; Peng, X. Recent development of chemosensors based on cyanine platforms. *Chem. Rev.* **2016**, *116*, 7768–7817. [[CrossRef](#)] [[PubMed](#)]
214. Shindy, H.A. Fundamentals in the chemistry of cyanine dyes: A review. *Dyes Pigment.* **2017**, *145*, 505–513. [[CrossRef](#)]
215. Johnson, J.R.; Fu, N.; Arunkumar, E.; Leevy, W.M.; Gammon, S.T.; Piwnica-Worms, D.; Smith, B.D. Squaraine rotaxanes: Superior substitutes for Cy-5 in molecular probes for near-infrared fluorescence cell imaging. *Angew. Chem. Int. Ed.* **2007**, *46*, 5528–5531. [[CrossRef](#)] [[PubMed](#)]

216. Podgorski, K.; Terpetschnig, E.; Klochko, O.P.; Obukhova, O.M.; Haas, K. Ultra-bright and -stable red and near-infrared squaraine fluorophores for in vivo two-photon imaging. *PLoS ONE* **2012**, *7*, e51980. [[CrossRef](#)] [[PubMed](#)]
217. Lavis, L.D. Teaching old dyes new tricks: Biological probes built from fluoresceins and rhodamines. *Ann. Rev. Biochem.* **2017**, *86*, 825–843. [[CrossRef](#)] [[PubMed](#)]
218. Kushida, Y.; Nagano, T.; Hanaoka, K. Silicon-substituted xanthene dyes and their applications in bioimaging. *Analyst* **2015**, *140*, 685–695. [[CrossRef](#)] [[PubMed](#)]
219. Ikeno, T.; Nagano, T.; Hanaoka, K. Silicon-substituted xanthene dyes and their unique photophysical properties for fluorescent probes. *Chem. Asian J.* **2017**, *12*, 1435–1446. [[CrossRef](#)] [[PubMed](#)]
220. Grimm, J.B.; Brown, T.A.; Tkachuk, A.N.; Lavis, L.D. General synthetic method for Si-fluorescein and Si-rhodamines. *ACS Cent. Sci.* **2017**, *3*, 975–985. [[CrossRef](#)] [[PubMed](#)]
221. Grimm, J.B.; Muthusamy, A.K.; Liang, Y.; Brown, T.A.; Lemon, W.C.; Patel, R.; Lu, R.; Macklin, J.J.; Keller, P.J.; Ji, N.; et al. A general method to fine-tune fluorophores for live-cell and in vivo imaging. *Nat. Methods* **2017**, *14*, 987–994. [[CrossRef](#)] [[PubMed](#)]
222. Zhou, X.; Lai, R.; Beck, J.R.; Li, H.; Stains, C.I. Nebraska Red: A phosphinate-based near-infrared fluorophore scaffold for chemical biology applications. *Chem. Commun.* **2016**, *52*, 12290–12293. [[CrossRef](#)] [[PubMed](#)]
223. Chai, X.; Cui, X.; Wang, B.; Yang, F.; Cai, Y.; Wu, Q.; Wang, T. Near-infrared phosphorus-substituted rhodamine with emission wavelength above 700nm for bioimaging. *Chem. Eur. J.* **2015**, *21*, 16754–16758. [[CrossRef](#)] [[PubMed](#)]
224. Bell, P.J.; Karuso, P. Epicocconone, a novel fluorescent compound from the fungus *epicoccum nigrum*. *J. Am. Chem. Soc.* **2003**, *125*, 9304–9305. [[CrossRef](#)] [[PubMed](#)]
225. Karuso, P.; Loa Kum Cheung, W.; Peixoto, P.A.; Boulangé, A.; Franck, X. Epicocconone-hemicyanine hybrids: Near infrared fluorophores for protein staining and cell imaging. *Chem. Eur.* **2017**, *23*, 1820–1829. [[CrossRef](#)] [[PubMed](#)]
226. Boulangé, A.; Peixoto, P.A.; Franck, X. Diastereoselective IBX oxidative dearomatization of phenols by remote induction: Towards the epicocconone core framework. *Chem. Eur.* **2011**, *17*, 10241–10245. [[CrossRef](#)] [[PubMed](#)]
227. Peixoto, P.A.; Boulangé, A.; Ball, M.; Naudin, B.; Alle, T.; Cosette, P.; Karuso, P.; Franck, X. Design and synthesis of epicocconone analogues with improved fluorescence properties. *J. Am. Chem. Soc.* **2014**, *136*, 15248–15256. [[CrossRef](#)] [[PubMed](#)]
228. Syzgantseva, O.A.; Tognetti, V.; Joubert, L.; Boulangé, A.; Peixoto, P.A.; Leleu, S.; Franck, X. Electronic excitations in epicocconone analogues: TDDFT methodological assessment guided by experiment. *J. Phys. Chem. A* **2012**, *116*, 8634–8643. [[CrossRef](#)] [[PubMed](#)]
229. Syzgantseva, O.A.; Tognetti, V.; Boulangé, A.; Peixoto, P.A.; Leleu, S.; Franck, X.; Joubert, L. Evaluating charge transfer in epicocconone analogue: Toward a targeted design of fluorophores. *J. Phys. Chem. A* **2014**, *118*, 757–764. [[CrossRef](#)] [[PubMed](#)]
230. Chatterjee, S.; Karuso, P.; Boulangé, A.; Peixoto, P.A.; Franck, X.; Datta, A. The role of different structural motifs in the ultrafast dynamics of second generation protein stains. *J. Phys. Chem. B* **2013**, *117*, 14951–14959. [[CrossRef](#)] [[PubMed](#)]
231. Chatterjee, S.; Karuso, P.; Boulangé, A.; Franck, X.; Datta, A. Excited states dynamics of brightly fluorescent second generation epicocconone analogues. *J. Phys. Chem. B* **2015**, *119*, 6295–6303. [[CrossRef](#)] [[PubMed](#)]
232. Hell, S.W.; Sahl, S.J.; Bates, M.; Zhuang, X.; Heintzmann, R.; Booth, M.J.; Bewersdorf, J.; Shtengel, G.; Hess, H.; Tinnefeld, P. The 2015 super-resolution microscopy roadmap. *J. Phys. Appl. Phys.* **2015**, *48*, 443001. [[CrossRef](#)]
233. Zheng, Q.F.; Juette, M.; Jockusch, S.R.; Wasserman, M.; Zhou, Z.B.; Altman, R.C.; Blanchard, S. Ultra-stable organic fluorophores for single-molecule research. *Chem. Soc. Rev.* **2014**, *43*, 1044–1056. [[CrossRef](#)] [[PubMed](#)]
234. Henderson, B.W.; Dougherty, T.J. How does photodynamic therapy work? *Photochem. Photobiol.* **1992**, *55*, 145–157. [[CrossRef](#)] [[PubMed](#)]
235. DeRosa, M.C.; Crutchley, R.J. Photosensitized singlet oxygen and its applications. *Coord. Chem. Rev.* **2002**, *233–234*, 351–371. [[CrossRef](#)]
236. Butkevich, A.N.; Mitronova, G.Y.; Sidenstein, S.C.; Klocke, J.L.; Kamin, D.; Meineke, D.N.H.; D'Este, E.; Kraemer, P.T.; Danzl, J.G.; Belov, V.N.; et al. Fluorescent rhodamines and fluorogenic carbopyronines for super-resolution STED microscopy in living cells. *Angew. Chem. Int. Ed.* **2016**, *55*, 3290–3294. [[CrossRef](#)] [[PubMed](#)]

237. Sreedharan, S.; Gill, M.R.; Garcia, E.; Saeed, H.K.; Robinson, D.; Byrne, A.; Cadby, A.; Keyes, T.E.; Smythe, C.; Pellett, P. Multimodal super-resolution optical microscopy using a transition-metal-based probe provides unprecedented capabilities for imaging both nuclear chromatin and mitochondria. *J. Am. Chem. Soc.* **2017**, *139*, 15907–15913. [[CrossRef](#)] [[PubMed](#)]
238. Lukinavičius, G.; Mitronova, Y.G.; Schnorrenberg, S.; Butkevich, A.N.; Barthel, H.; Belov, V.N.; Hell, S.W. Fluorescent dyes and probes for super-resolution microscopy of microtubules and tracheoles in living cells and tissues. *Chem. Sci.* **2018**, *9*, 3324–3334. [[CrossRef](#)] [[PubMed](#)]
239. Butkevich, A.N.; Ta, H.; Ratz, M.; Stoldt, S.; Jakobs, S.; Belov, V.N.; Hell, S.W. Two-Color 810 nm STED nanoscopy of living cells with endogenous SNAP-tagged fusion proteins. *ACS Chem. Biol.* **2018**, *13*, 475–480. [[CrossRef](#)] [[PubMed](#)]
240. Thompson, A.D.; Bewersdorf, J.; Toomre, D.; Schepartz, A. HIDE probes: A new toolkit for visualizing organelle dynamics, longer and at super-resolution. *Biochemistry* **2017**, *56*, 5194–5201. [[CrossRef](#)] [[PubMed](#)]
241. Saurabh, S.; Perez, A.M.; Commerci, C.J.; Shapiro, L.; Moerner, W.E. Super-resolution imaging of live bacteria cells using a genetically directed, highly photostable fluoromodule. *J. Am. Chem. Soc.* **2016**, *138*, 10398–10401. [[CrossRef](#)] [[PubMed](#)]
242. Kolmakov, K.; Wurm, C.A.; Hennig, R.; Rapp, E.; Jakobs, S.; Belov, V.N.; Hell, S.W. Red-emitting rhodamines with hydroxylated, sulfonated, and phosphorylated dye residues and their use in fluorescence nanoscopy. *Chem. Eur. J.* **2012**, *18*, 12986–12998. [[CrossRef](#)] [[PubMed](#)]
243. Nizamov, S.; Sednev, M.V.; Bossi, M.L.; Heibisch, E.; Frauendorf, H.; Lehnart, S.E.; Belov, V.N.; Hell, S.W. “Reduced” coumarin dyes with an O-phosphorylated 2,2-dimethyl-4-(hydroxymethyl)-1,2,3,4-tetrahydroquinoline fragment: Synthesis, spectra, and STED microscopy. *Chem. Eur. J.* **2016**, *22*, 11631–11642. [[CrossRef](#)] [[PubMed](#)]
244. Wang, C.; Fukazawa, A.; Taki, M.; Sato, Y.; Higashiyama, T.; Yamaguchi, S. A phosphole oxide based fluorescent dye with exceptional resistance to photobleaching: A practical tool for continuous imaging in STED microscopy. *Angew. Chem. Int. Ed.* **2015**, *54*, 15213–15217. [[CrossRef](#)] [[PubMed](#)]
245. Yang, S.K.; Shi, X.; Park, S.; Ha, T.; Zimmerman, S.C. A dendritic single-molecule fluorescent probe that is monovalent, photostable and minimally blinking. *Nat. Chem.* **2013**, *5*, 692–697. [[CrossRef](#)] [[PubMed](#)]
246. Van der Velde, J.H.M.; Ploetz, E.; Hiermaier, M.; Oelerich, J.; de Vries, J.W.; Roelfes, G.; Cordes, T. Mechanism of intramolecular photostabilization in self-healing cyanine fluorophores. *Chem. Phys. Chem.* **2013**, *14*, 4084–4093. [[CrossRef](#)] [[PubMed](#)]
247. Cortés, E.; Huidobro, P.A.; Sinclair, H.G.; Guldbrand, S.; Peveler, W.J.; Davies, T.; Parrinello, S.; Görlitz, F.; Dunsby, C.; Neil, M.A.A.; et al. Plasmonic nanoprobe for Stimulated Emission Depletion nanoscopy. *ACS Nano* **2016**, *10*, 10454–10461. [[CrossRef](#)] [[PubMed](#)]
248. Lord, S.J.; Conley, N.R.; Lee, H.D.; Samuel, R.; Liu, N.; Twieg, R.J.; Moerner, W.E. A photoactivatable push–pull fluorophore for single-molecule imaging in live cells. *J. Am. Chem. Soc.* **2008**, *130*, 9204–9205. [[CrossRef](#)] [[PubMed](#)]
249. Dempsey, G.T.; Bates, M.; Kowtoniuk, W.E.; Liu, D.R.; Tsien, R.Y.; Zhuang, X. Photoswitching mechanism of cyanine dyes. *J. Am. Chem. Soc.* **2009**, *131*, 18192–18193. [[CrossRef](#)] [[PubMed](#)]
250. Heilemann, M.; Margeat, E.; Kasper, R.; Sauer, M.; Tinnefeld, P. Carbocyanine dyes as efficient reversible single-molecule optical switch. *J. Am. Chem. Soc.* **2005**, *127*, 3801–3806. [[CrossRef](#)] [[PubMed](#)]
251. Dempsey, G.T.; Vaughan, J.C.; Chen, K.H.; Bates, M.; Zhuang, X. Evaluation of fluorophores for optimal performance in localization-based super-resolution imaging. *Nat. Methods* **2011**, *8*, 1027–1036. [[CrossRef](#)] [[PubMed](#)]
252. Minoshima, M.; Kikuchi, K. Photostable and photoswitching fluorescent dyes for super-resolution imaging. *J. Biol. Inorg. Chem.* **2017**, *22*, 639–652. [[CrossRef](#)] [[PubMed](#)]
253. Roubinet, B.; Weber, M.; Shojaei, H.; Bates, M.; Bossi, M.L.; Belov, V.N.; Irie, M.; Hell, S.W. Fluorescent photoswitchable diarylethenes for biolabeling and single-molecule localization microscopies with optical superresolution. *J. Am. Chem. Soc.* **2017**, *139*, 6611–6620. [[CrossRef](#)] [[PubMed](#)]
254. Rodriguez, P.C.; Pereira, D.B.; Borgkvist, A.; Wong, M.Y.; Barnard, C.; Sonders, M.S.; Zhang, H.; Sames, D.; Sulzer, D. Fluorescent dopamine tracer resolves individual dopaminergic synapses and their activity in the brain. *Proc. Natl. Acad. Sci. USA* **2013**, *110*, 870–875. [[CrossRef](#)] [[PubMed](#)]
255. Yu, Z.; Ohulchanskyy, T.Y.; An, P.; Prasad, P.N.; Lin, Q. Fluorogenic, two-photon-triggered photoclick chemistry in live mammalian cells. *J. Am. Chem. Soc.* **2013**, *135*, 16766–16769. [[CrossRef](#)] [[PubMed](#)]

256. Jing, C.; Cornish, V.W. A fluorogenic TMP-tag for high signal-to-background intracellular live cell imaging. *ACS Chem. Biol.* **2013**, *8*, 1704–1712. [CrossRef] [PubMed]
257. Pimenta, F.M.; Chiappetta, G.; Le Saux, T.; Vinh, J.; Jullien, L.; Gautier, A. Chromophore renewal and fluorogen-binding tags: A match made to last. *Sci. Rep.* **2017**, *7*, 12316. [CrossRef] [PubMed]
258. Marx, V. Is super-resolution microscopy right for you? *Nat. Methods* **2013**, *10*, 1157–1163. [CrossRef] [PubMed]
259. Webb, S.E.; Zanetti-Domingues, L.; Coles, B.C.; Rolfe, D.J.; Wareham, R.J.; Martin-Fernandez, M.L. Multicolour single molecule imaging on cells using a supercontinuum source. *Biomed. Opt. Express* **2012**, *3*, 400–406. [CrossRef] [PubMed]
260. Khanna, V.K. LEDs, OLEDs, and their applications in illumination and displays. In *Fundamentals of Solid-State Lighting*; Taylor & Francis Group, Ed.; CRC Press: London, UK, 2014.
261. So, P.T.; Masters, B.R.; Berland, K.M. Two-photon excitation fluorescence microscopy. *Annu. Rev. Biomed. Eng.* **2000**, *2*, 399–429. [CrossRef] [PubMed]
262. Graf, R.; Rietdorf, J.; Zimmerman, T. Live cell spinning disk microscopy. *Adv. Biochem. Eng./Biotechnol.* **2005**, *95*, 57–75.
263. Bethge, P.; Chéreau, R.; Avignone, E.; Marsicano, G.; Nägerl, U.V. Two-photon excitation STED microscopy in two colors in acute brain slices. *Biophys. J.* **2013**, *104*, 778–785. [CrossRef] [PubMed]
264. Godin, A.G.; Lounis, B.; Cognet, L. Super-resolution microscopy approaches for live cell imaging. *Biophys. J.* **2014**, *107*, 1777–1784. [CrossRef] [PubMed]
265. Martini, N.; Bewersdorf, J.; Hell, S.W. A new high-aperture glycerol immersion objective lens and its application to 3D-fluorescence microscopy. *J. Microsc.* **2002**, *206*, 146–151. [CrossRef] [PubMed]
266. Gregor, I.; Enderlein, J. Focusing astigmatic Gaussian beams through optical systems with a high numerical aperture. *Opt. Lett.* **2005**, *30*, 2527–2529. [CrossRef] [PubMed]
267. Geusebroek, J.M.; Cornelissen, F.; Smeulders, A.; Geerts, H. Robust autofocus in microscopy. *Cytometry* **2000**, *39*, 1–9. [CrossRef]
268. Bénard, M.; Lebon, A.; Komuro, H.; Vaudry, D.; Galas, L. Ex vivo imaging of postnatal cerebellar granule cell migration using confocal macroscopy. *J. Vis. Exp.* **2015**, *99*, e52810. [CrossRef] [PubMed]
269. Quan, T.; Zeng, S.; Huang, Z. Localization capability and limitation of electron-multiplying charge-coupled, scientific complementary metal-oxide semiconductor, and charge-coupled devices for super-resolution imaging. *J. Biomed. Opt.* **2010**, *15*, 066005. [CrossRef] [PubMed]
270. DeWeert, M.J.; Cole, J.B.; Sparks, A.W.; Acker, A. Photon transfer methods and results for electron multiplication CCDs. *Proc. SPIE* **2004**, *5558*, 248–259.
271. Coates, C.G.; Denvir, D.J.; Conroy, E.; McHale, N.G.; Thornbury, K.; Hollywood, M. Back-illuminated electron multiplying technology: The world's most sensitive CCD for ultralow-light microscopy. In *Manipulation and Analysis of Biomolecules, Cells, and Tissues*; Nicolau, D.V., Enderlein, J., Leif, R.C., Farkas, D.L., Eds.; Int. Soc. Optical Engineering: Bellingham, WA, USA, 2003; Volume 4962, pp. 319–328.
272. To See or Not to See. Can Non-Cooled sCMOS Cameras Do the Job? Available online: <https://www.imaging-git.com/applications/see-or-not-see> (accessed on 13 September 2018).
273. Zucker, R.M. Quality assessment of confocal microscopy slide-based systems: Instability. *Cytometry A* **2006**, *69*, 659–676. [CrossRef] [PubMed]
274. Adler, J.; Pagakis, S.N. Reducing image distortions due to the temperature-related microscope stage drift. *J. Microsc.* **2003**, *210*, 131–137. [CrossRef] [PubMed]
275. Arbelle, A.; Reyes, J.; Chen, J.Y.; Lahav, G.; Riklin Raviv, T.A. Probabilistic approach to joint cell tracking and segmentation in high-throughput microscopy videos. *Med. Image Anal.* **2018**, *47*, 140–152. [CrossRef] [PubMed]
276. Helmuth, J.A.; Burckhardt, C.J.; Koumoutsakos, P.; Greber, U.F.; Sbalzarini, I.F. A novel supervised trajectory segmentation algorithm identifies distinct types of human adenovirus motion in host cells. *J. Struct. Biol.* **2007**, *159*, 347–358. [CrossRef] [PubMed]
277. Cordelières, F.P.; Petit, V.; Kumasaka, M.; Debeir, O.; Letort, V.; Gallagher, S.J.; Larue, L. Automated cell tracking and analysis in phase-contrast videos (iTrack4U): Development of Java software based on combined mean-shift processes. *PLoS ONE* **2013**, *8*, e81266.

